Microporous and Mesoporous Materials 381 (2025) 113371

Contents lists available at ScienceDirect

Microporous and Mesoporous Materials

journal homepage: www.elsevier.com/locate/micromeso

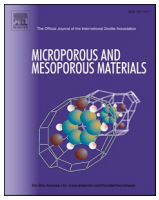

Non-hydrolytic sol-gel synthesis of amine-functionalized silica: Template- and catalyst-free preparation of mesoporous catalysts for CO_2 valorization

Thai Q. Bui [a], Tomas Pokorny [a], Petr Machac [a], Zdenek Moravec [a], Eva Domincova Bergerova [b], Ales Styskalik [a,*]

[a] Department of Chemistry, Faculty of Science, Masaryk University, Kotlarska 2, CZ-61137 Brno, Czech Republic
[b] Centre of Polymer Systems, Tomas Bata University in Zlin, tr. Tomase Bati 5678, CZ-76001, Zlin, Czech Republic

ARTICLE INFO

Keywords:
Non-aqueous condensation
Silsesquioxane
Tertiary amine
Heterogeneous catalysis
Carbon dioxide
Epoxide
Cyclic carbonate

ABSTRACT

Carbon dioxide utilization presents an important and topical research topic. However, the performance of catalysts needed for CO_2 transformations does not achieve the necessary levels for their widespread application. To this end, we decided to study non-aqueous condensations providing amine-functionalized silica catalysts, possibly active in CO_2-epoxide cycloaddition reaction. While non-hydrolytic sol-gel method is well-known for its efficiency in providing highly porous Lewis and Brønsted acid metallosilicates, here we show for the first time its application for the preparation of silica-based catalysts containing basic groups. First, the reaction conditions were screened to reproducibly obtain porous materials with preserved amine moieties. These were identified as follows: silicon tetraacetate and bridging tertiary amine silanes as precursors, toluene as a solvent, and temperature between 160 and 180 °C. In such a way, materials with up to 776 $m^2\ g^{-1}$ and 1.58 $cm^3\ g^{-1}$ were obtained in one-step process, without any template, after conventional drying step. Next, the amine-functionalized materials were tested in CO_2-epoxide coupling providing cyclic organic carbonates with high selectivity (>99 %) and moderate activity (up to 86 % epichlorohydrin conversion after 1 h at 120 °C and 10 bar CO_2). The characterization of spent catalysts revealed a presence of cyclic organic carbonates at the catalyst surface as well as conversion of tertiary amine groups to quaternary ammonium moieties.

1. Introduction

Organic-inorganic hybrid materials (OIHMs) have been studied extensively in both academia and industry because they can be tailored to possess desirable properties to suit a wide range of applications thanks to possibility to combine the versatility of organic species with the advantages of inorganic components such as excellent thermal stability and robust structure [1]. Generally, OIHMs can be classified into two major classes depending on the nature of interactions between organic and inorganic phases. Class I hybrids contain weak interactions (van der Waals, π–π, hydrogen bonding, electrostatic) while class II hybrids contain strong (covalent) bonds between two constituents.

In the field of heterogeneous catalysis, class II hybrids are preferable to class I ones because strong bonds between organic and inorganic building blocks in the former would favor preservation of the hybrid catalysts during catalytic reaction, minimizing leaching of the active organic moiety into reaction media [2]. Mesoporous silica-based hybrids derived from the sol-gel synthesis method are particularly attractive as potential hybrid heterogeneous catalysts due to the wide availability of organosilicon precursors in the market, the ease of preparation and tuning as well as the high accessibility of active sites and the efficient mass transport [2]. So far, these hybrids have been synthesized mainly by using the traditional sol-gel method, *aka* the hydrolytic sol-gel (HSG), whose mechanism is related to hydrolysis and polycondensation reactions. However, there are two major limitations in this method when water is used as a solvent [3]. First, different metal/silicon precursors (e.g., $Si(OR)_4$ vs. $Ti(OR)_4$ or $Si(OR)_4$ vs. $R'_xSi(OR)_{4-x}$) may have significantly different hydrolysis as well as polycondensation rates under aqueous conditions leading to phase separation or heterogeneity. Second, due to high surface tension of water, the pore structures of wet gel may collapse during the drying process resulting in materials with poor textural properties.

To overcome the limitations of the HSG mentioned above, the non-hydrolytic sol-gel (NHSG) can be seen as an alternative method where

* Corresponding author.
E-mail address: styskalik@chemi.muni.cz (A. Styskalik).

https://doi.org/10.1016/j.micromeso.2024.113371
Received 2 August 2024; Received in revised form 9 October 2024; Accepted 11 October 2024
Available online 12 October 2024

the sol-gel processes take place in water-free environments. The NHSG method relies on non-hydrolytic polycondensation reactions between metal/silicon precursors and oxygen donors other than water under non-aqueous conditions and leads to the formation of metal/silicon oxides [3,4]. On one hand, such approach brings several difficulties and environmental concerns including application of organic solvents, lengthy procedures, and work under dry N_2 atmosphere (either in the glovebox and/or applying the N_2/vacuum manifold). However, these downfalls are counterbalanced by decisive advantages. First, The condensation reaction rates are usually lower and levelled off compared to ones under aqueous environments, leading to the formation of materials with well-controlled properties such as homogeneity, composition, morphology, texture, and surface chemistry. Second, a conventional gel drying provides often highly porous materials. Organic solvents exhibit much lower surface tension in comparison to water and therefore the application of templates or supercritical/freeze drying is not necessary. Thanks to these advantages (but not limited to), materials prepared from the NHSG method have found many applications in industry such as heterogeneous catalysts, luminescent materials, catalyst supports, and Li-ion battery electrodes [3,5].

In the field of heterogeneous catalysis, the NHSG method is particularly beneficial for the preparation of mesoporous mixed oxide catalysts compared to the HSG method in terms of simplicity, versatility, and properties control [6,7]. In addition, this method could also be useful for the preparation of organic-inorganic hybrid catalysts [8]. However, to the best of our knowledge, only mixed oxide catalysts functionalized with alkyl and/or aryl groups have been so far reported as class II hybrid catalysts prepared by the NHSG method [8–16]. Therefore, it is still in its infancy and, indeed, needs more efforts to exploit further the potential of the NHSG method in the preparation of class II hybrid materials, particularly in the field of heterogeneous catalysis.

One way of broadening their spectra of class II hybrid catalysts derived from the NHSG method is through the introduction of amine groups into inorganic materials structure. Amine is one of the most attractive organic functional groups due to its wide applications. Particularly, tertiary amines and heterocyclic amines are promising metal- and halogen-free organocatalysts for the synthesis of cyclic organic carbonates from CO_2 and epoxides [17–21]. This cycloaddition reaction is one of the most promising routes for chemical fixation of CO_2 on industrial scale due to 100 % atom economy and producing valuable cyclic carbonate products. While homogeneous catalysts provide excellent catalytic activity, heterogeneous catalysts are technically preferable in industry due to the ease of catalyst separation and recycling as well as the ease of application in continuous-flow processes. Several types of heterogeneous catalysts containing nitrogen-amine active sites for this reaction have been successfully developed such as N-doped carbons [22], mesoporous melamine-formaldehyde resins [23], covalent organic frameworks (COFs) [24], metal-organic frameworks (MOFs) [25], poly(ionic liquid)s (PILs) [26], and mesoporous amine-silica hybrids [27–29]. Among them, mesoporous amine-silica hybrids are particularly attractive due to metal- and halogen-free nature, low-cost, simple preparation, efficient mass transport, and robust structure. So far, mesoporous amine-silica catalysts for the cycloaddition reaction have been prepared mainly by grafting amine precursors on mesoporous silica supports [27–29]. Although this post-modification method exhibited considerable success in the preparation of mesoporous amine-silica catalysts, an effective and simple one-pot synthesis (*aka* direct synthesis) is highly desired. In this regard, the use of bridged trialkoxysilylated amine precursors for direct sol-gel synthesis of mesoporous amine-silica hybrids is highly promising. Several mesoporous amine-silica hybrids derived from bridged trialkoxysilylated amine precursors showed high porosity, high thermostability, high content of surface amine groups [30–32], and were applied in several applications such as heterogeneous organocatalysts [33,34], CO_2 adsorbents [35–37], perfluorinated compounds adsorbents [38], Hg(II) adsorbents [39], and dyes adsorbents [40]. However, there is little information about applying these materials for the cycloaddition reaction between epoxides and CO_2. In addition, these materials have been prepared mainly via traditional hydrolytic sol-gel and using structure-directing agents to create mesopores (Table S1).

In this report, we applied a template-free and one-pot NHSG method to co-condense mono/bis/tris-trimethoxysilylated amine precursors bearing aliphatic amine moieties with silica precursors ($SiCl_4$ and $Si(OAc)_4$). Our aim was to prepare mesoporous amine-silica class II hybrids as potential metal- and halogen-free catalysts for the CO_2-epoxide cycloaddition reaction. First, the ideal reaction conditions were unambiguously identified. Second, the structure and the adsorption properties of the resulting materials were described in detail. Finally, the comparison of catalytic performance of amine-silica materials with their homogeneous analogues as well as characterization of spent catalysts revealed an interesting behavior of heterogeneous catalysts prepared by NHSG polycondensation.

2. Experimental

General information is written in Supporting Information.

2.1. Synthesis of hybrid amine-silica xerogels

Novel hybrid amine-silica materials were prepared in one pot using non-hydrolytic sol-gel (NHSG) method, specifically via alkyl halide and ester elimination routes [3,5]. The structures of amine and silica precursors in this study are presented in Fig. 1. Anhydrous dichloromethane (DCM), tetrahydrofurane (THF), and toluene (TOL) were used as solvents.

Typically, we mixed 3 g of a silica precursor SiX_4 ($X = CH_3COO$ or Cl) with 10 mL of an aprotic solvent (DCM/THF/TOL) in a Teflon-lined stainless-steel autoclave (100 mL) under N_2 atmosphere in a dry box. Subsequently, we added to the mixture a stoichiometric amount of an amine precursor (Equations (1)—4, Fig. 1), which contains either a terminal primary amine group (denoted as N1) or a bridging secondary/tertiary amine group (denoted as N2/N3-Me/N3). The resulting mixture was magnetically stirred until we got a clear solution. Next, the autoclave was sealed and aged at a desired temperature (140—200 °C) in an oven for 4 days under autogenous pressure. After this, the autoclave was cooled to room temperature and then opened inside a dry box. The obtained gel was crushed, transferred to a Schlenk vessel, and dried under vacuum at 120 °C overnight to remove volatile products (e.g., CH_3X) and solvent. The volatile products were identified by using GC-MS.

$$3\ SiX_4 + 4\ (CH_3O)_3Si(CH_2)_3NH_2\ \textbf{(N1)} \rightarrow 12\ CH_3X + Si_7O_{12}(CH_2)_{12}(NH_2)_4 \quad \text{(eq. 1)}$$

$$3\ SiX_4 + 2\ [(CH_3O)_3Si(CH_2)_3]_2NH\ \textbf{(N2)} \rightarrow 12\ CH_3X + Si_7O_{12}(CH_2)_{12}(NH)_2 \quad \text{(eq. 2)}$$

$$3\ SiX_4 + 2\ [(CH_3O)_3Si(CH_2)_3]_2NCH_3\ \textbf{(N3-Me)} \rightarrow 12\ CH_3X + Si_7O_{12}(CH_2)_{12}(NCH_3)_2 \quad \text{(eq. 3)}$$

$$9\ SiX_4 + 4\ [(CH_3O)_3Si(CH_2)_3]_3N\ \textbf{(N3)} \rightarrow 36\ CH_3X + Si_{21}O_{36}(CH_2)_{36}N_4 \quad \text{(eq. 4)}$$

3. Results and discussion

3.1. Ester elimination route: The NHSG condensation and porosity of hybrid materials

In this route, $Si(OAc)_4$ was used as a silica precursor together with 4 amine precursors (N1/N2/N3-Me/N3) containing trimethoxysilyl groups to synthesize hybrid amine-silica materials (Equations (1)—4).

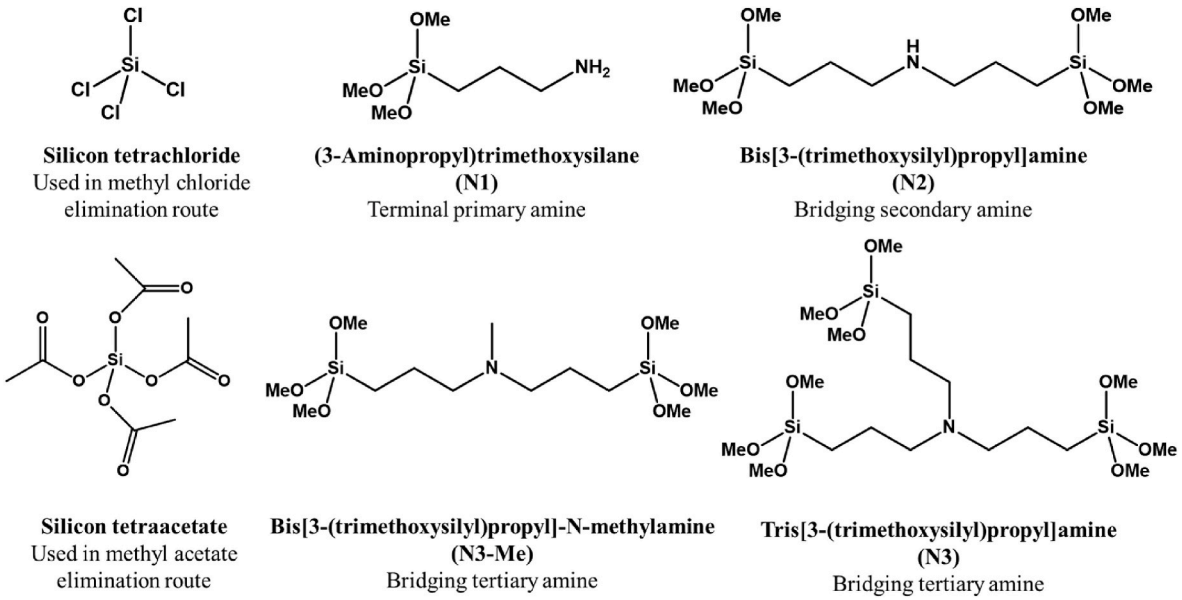

Fig. 1. Chemical structures of silica and amine precursors in this study.

The silica and amine precursors were mixed with an equal number of acetoxy and methoxy functional groups in an aprotic solvent. The presence of methyl acetate as a volatile product in all synthesis experiments was confirmed by GC-MS analysis of residue solvents after the non-hydrolytic sol-gel (NHSG) synthesis. The so-called ester elimination has been reported to provide a broad variety of materials including silicophosphates [41], their hybrid derivatives [42], metallosilicates [43,44], and metal trimethylsiloxides [45]. While Lewis acidity of the metal centers has usually been reported to drive the NHSG condensation [45], such sites are lacking in our case. Based on the fact that there was no gelation between $Si(OAc)_4$ and trimethoxymethylsilane $CH_3Si(OCH_3)_3$ under similar synthesis conditions (10 mL of DCM, 180 °C, 4 days), we believe that N-sites from amine precursors could play a role as a catalyst for the NHSG synthesis of amine-functionalized silicas.

It should be noted that carboxylic acid esters (i.e., methyl acetate, silicon tetraacetate) can react with primary and secondary amines forming secondary and tertiary amides, respectively [27,46]. This reaction should be accompanied by methanol formation. GC-MS analysis confirmed MeOH presence in residue volatiles after NHSG syntheses when applying N1 and N2 precursors. Therefore, the possible amide formation was carefully checked (see section 3.2 Ester elimination route: The structure of hybrid materials).

The N_2 adsorption–desorption isotherms and corresponding NLDFT pore size distributions of some selected hybrid xerogels obtained from the ester elimination route under different conditions (amine precursor, aprotic solvent, temperature) are given in Fig. S1. The isotherms adopt type IV typical for mesoporous materials (except for sample N1 which was non-porous, see discussion below). The hysteresis loops are mostly H2-type indicating the presence of irregular mesopores with complex pore structures [47]. Some samples exhibit steep N_2 adsorption at $p/p_0 > 0.9$ indicating the presence of interparticle voids [47]. Indeed, the NLDFT models (Fig. S1, right) show pore sizes ranging in the mesopore region (and to some extent in the macropore region) over tens of nanometers as can be expected for the NHSG synthesis applying no templating agents. The qualitative N_2 adsorption-desorption isotherms evaluation agrees well with the morphology of the materials observed by SEM and TEM (Figs. S2 and S3). The micrographs show irregular sponge-like particles with sizes in the micron range that appear to contain both meso- and macropores.

Table 1 summarizes the quantitative textural properties of hybrid amine-silica materials synthesized from the ester elimination route under different synthetic conditions (amine precursor, aprotic solvent,

Table 1
Textural properties of hybrid amine-silica xerogels obtained from the ester elimination route ($Si(OAc)_4$ as a silica precursor) under different conditions.

Gel	Amine precursor	Aprotic solvent	Temp. (°C)	S_{BET} ($m^2\ g^{-1}$)	[a]V_{total} ($cm^3\ g^{-1}$)	[b]$V_{micro}/V_{tot.}$ (%)	[c]PS_{DFT} (nm)	[d]$PS_{aver.}$ (nm)
1	N1	TOL	180	<10	n.d.[e]	n.d.	n.d.	n.d.
2	N2	DCM	180	664	0.43	12.6	2.6	2.6
3		THF	180	708	1.18	4.2	10.5	6.7
4		TOL	180	624	1.32	3.1	7.0	8.5
5		TOL	160	426	0.53	3.6	6.6	5.0
6	N3-Me	DCM	180	604	0.58	2.9	2.6	3.8
7		THF	180	700	0.63	9.0	2.6	3.6
8		TOL	200	303	0.92	1.0	29.4	12.2
9		TOL	180	776	1.58	0.7	13.9	8.1
10		TOL	160	666	0.93	1.9	3.2	5.6
11		TOL	140	141	0.47	0.0	7.0	13.2
12	N3	TOL	180	761	1.26	2.7	6.8	6.6
13		TOL	140	396	0.61	0.5	6.8	6.1

[a] Estimated at $p/p_o = 0.97$.
[b] Based on t-plot analyses (Fig. S4).
[c] The maximum value of the pore size distribution curve (NLDFT, ads, cyl. pore model).
[d] $4V_{total}/S_{BET}$.
[e] Not determined.

temperature). It is clearly seen from Table 1 that materials derived from bridging amine precursors (N2/N3-Me/N3) often exhibited high specific surface areas (S_{BET}; 141—776 $m^2\ g^{-1}$), high total pore volumes (V_{total}; 0.43—1.58 $cm^3\ g^{-1}$), and large mesopores. All three bridging amine precursors (N2/N3-Me/N3) reacted with $Si(OAc)_4$ at different temperatures and in various solvents. The comparison of both S_{BET} and V_{total} clearly highlights 180 °C as the ideal synthetic temperature; specific surface areas and total pore volumes are lower at both higher (200 °C) and lower (140 °C, 160 °C) temperatures (Table 1). This observation is probably connected with the condensation degree: the materials synthesized at 180 °C exhibit only low signals of unreacted organic groups and, at the same time, no signs of decomposition (see section 3.2 Ester elimination route: Structure of hybrid materials). Regarding the effect of solvents on porosity, materials synthesized in dichloromethane (DCM), tetrahydrofuran (THF), and toluene exhibited similar S_{BET} ranging from 604 to 776 $m^2\ g^{-1}$. However, the V_{total} was always significantly higher in nonpolar toluene than in polar DCM or THF (Table 1).

In contrary to samples prepared with bridging amine precursors (N2/N3-Me/N3), the material derived from the terminal amine precursor (N1) was non-porous (S_{BET} < 10 $m^2\ g^{-1}$) under template/additive/catalyst-free and NHSG synthesis conditions. This observation agrees with reported results from NHSG synthesis of hybrid silicophosphate xerogels [42]. Specifically, the co-condensation reactions between $Si(OAc)_4$ and terminal precursors $R—P(O)(OSiMe_3)_2$ (R = alkyl or aryl group) produced non-porous materials while the co-condensation reactions between $Si(OAc)_4$ and bridged ones $(Me_3SiO)_2(O)P—R—P(O)(OSiMe_3)_2$ produced highly porous materials (553—617 $m^2\ g^{-1}$). Similar results were also observed from the use of terminal and bridged silane precursors ($MeSi(OAc)_3$ *vs.* $(AcO)_3Si—R—Si(OAc)_3$, respectively) with tris(trimethylsilyl)phosphate $P(O)(OSiMe_3)_3$ [42]. The improved porosity when applying bridging precursors comes from the additional cross-linking introduced by the organic bridge, while the organosilane precursors with terminal organic groups provide, in fact, a lower connectivity in comparison to both bridged and convenient (i.e., four-connected) silica precursors [42].

To the best of our knowledge, there is no report related to using N1/N2/N3-Me/N3 amine precursors in the template/additive/catalyst-free and NHSG synthesis of hybrid amine-silica materials. Most importantly, even without using any template/additive/catalyst, the mesoporous materials (with a clear hysteresis loop) derived from bridging amine precursors (N2/N3-Me/N3) using NHSG exhibited comparable or even better textural properties compared to the ones using hydrolytic sol-gel (HSG) approach (Table S1).

3.2. Ester elimination route: The structure of hybrid materials

In order to confirm the structural integrity of organic moieties before and after NHSG synthesis under different conditions, we performed solid-state ^{13}C CP MAS NMR measurements for the hybrid amine-silica xerogels and compared the results with liquid-state ^{13}C NMR (in $CDCl_3$) spectra of their corresponding amine precursors. The results show that the synthesis performed in toluene at 180 °C was the optimum condition in our study to preserve the organic structure of the amine precursors in their corresponding hybrid xerogels (Fig. 2, S5, S6) [30]. The additional signal at ~170 ppm represents carbonyl groups in residual acetoxy or acetamide groups (see explanation below) [41]. The signal of corresponding methyl groups (22.6 ppm in silicon tetraacetate [41]) is overlapping with signals coming from methylene moieties in amine precursors. From Fig. S5 we can clearly see "unusual" peaks in ^{13}C CP MAS NMR spectra of materials synthesized in DCM, especially in the case of N3-Me precursor, compared to ones synthesized in TOL or THF. The possible reasons for this observation could be due to side reactions between amine sites and DCM under synthetic conditions [48]. Similar patterns were observed in alkyl halide elimination (CH_3Cl produced as volatile product) and in spent catalysts (reaction with epichlorohydrin and/or [4-(chloromethyl)-1,3-dioxolan-2-one]) and were explained by occurrence of side reactions on amine sites, i.e., quaternization, reverse Menschutkin, and Hofmann reactions (see section 3.6 Recyclability studies and spent catalysts characterization) [48–51].

Regarding the effect of temperature, it can be seen from Fig. S6 that intensities of methoxy and acetoxy groups decrease when the synthetic temperature increases from 140 to 180 °C, indicating a higher degree of co-condensation. However, the appearance of unwanted peaks at 65 ppm and 26 ppm together with the significant reducing of intensities of signals at 63 ppm and 45 ppm indicate decomposition of organic moieties in toluene at 200 °C (Fig. S6). This observation also agrees with the N_2 physisorption results in which the hybrid xerogels synthesized in toluene at 180 °C showed the optimum textural properties (Table 1).

Importantly, the quantitative ^{29}Si MAS NMR spectra (Fig. 3) of 4 hybrid materials synthesized under optimum conditions show that there was a great agreement between the experimental vs. theoretical ratio T-type silicon atoms over Q-type silicon atoms (theoretical ratio T/Q = 4/3 or 1.33), indicating the validity of proposed co-condensation reactions (Equations (1)—4).

Results from the thermogravimetric analysis (TGA) show that these hybrid amine-silica materials started to decompose at around 200—225 °C under air flow (Fig. S7a) while they were stable up to around 350 °C under N_2 flow (Fig. S7b). These observations indicate the

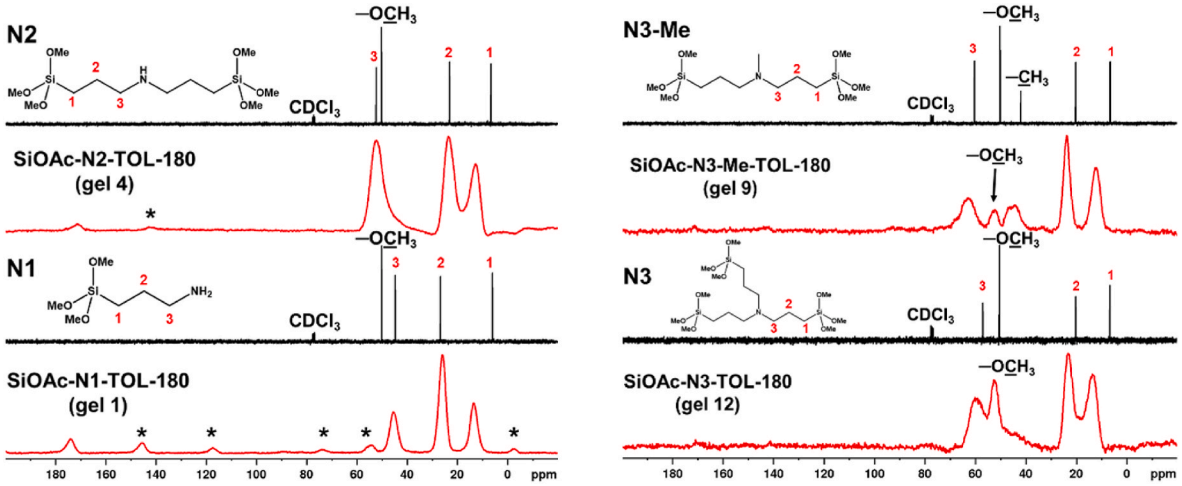

Fig. 2. Solid-state ^{13}C CP MAS NMR spectra of 4 representative hybrid materials synthesized under optimum conditions (toluene, 180 °C) from the ester elimination route and liquid-state ^{13}C NMR (in $CDCl_3$) spectra of their corresponding amine precursors. Asterisk mark denotes rotational sidebands.

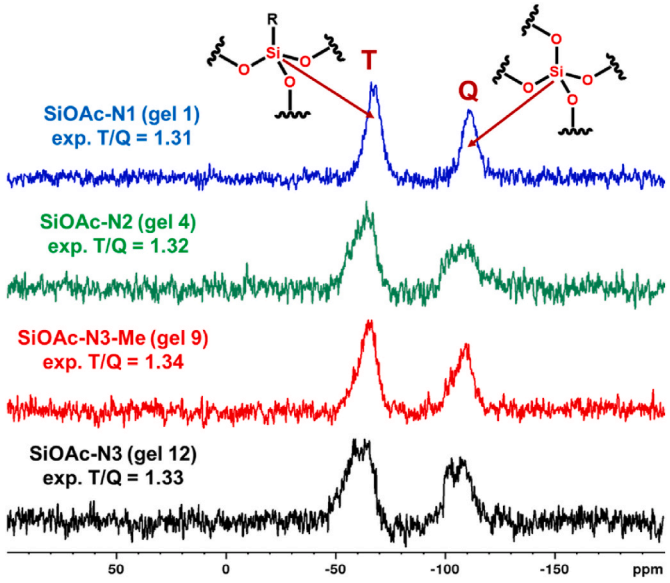

Fig. 3. Solid-state ^{29}Si MAS NMR (one pulse) spectra of 4 representative hybrid materials synthesized under optimum conditions (toluene, 180 °C) from the ester elimination route.

presence of organic functional groups in the xerogel structure. We assumed that, first, residue solids at the end of TGA experiments (till 1000 °C) under air flow were composed of SiO_2 only (Fig. S7a) and, second, all Si and N atoms from silica and amine precursors were transferred completely to final hybrid xerogels (Equations (1)—4). It should be noted that Equations (1)–(4) are ideal equations where the degrees of condensation (DC) are 100 %. In our second assumption, the real DC (<100 %) does not affect the Si/N molar ratio in the final gel because with different values of DC, the final gel will only have different amount of unreacted methoxy and acetoxy groups (ester elimination route). Based on our 2 assumptions, we calculated N contents of representative hybrid xerogels based on TGA results performed in air and presented them in Table 2. An example of our calculations for N content of SiOAc-N3 is provided in the Supporting Information. Interestingly, these calculated values of N content agreed very well with experimental values obtained from organic elemental analysis (Table 2), indicating the validity of our assumptions as well as agreement with the structural integrity of organic moieties from solid-state NMR results mentioned above (Figs. 2 and 3). Calculated Si contents of hybrid xerogels and mass loss values obtained from TGA-Air are presented in Table S2.

XPS and FT-IR measurements were further conducted to determine the surface elemental compositions and structural units of the hybrid amine-silica materials. The survey scan XPS spectra (not shown) revealed the appearance of 4 elements (Si, N, C, and O) on the surface of these materials, indicating the presence of hybrid organic-inorganic structure. The high-resolution XPS profiles of their Si2p, N1s, C1s, and O1s branches are shown in Fig. 4. The Si2p spectra (Fig. 4a) show 2 major peaks at binding energies (BE) ~102.7 and ~103.6 eV corresponding to Q-type silicon (SiO_4) and T-type silicon (SiO_3C) configurations, respectively [52,53]. It should be noted that the T/Q ratio in Si2p spectra was set to 1.33 to be consistent with the theoretical T/Q ratio in bulk materials when performing the curve-fitting by using CasaXPS software. The N1s spectra (Fig. 4b) show that the main N-species in 2 materials SiOAc-N3 and SiOAc-N3-Me was amine-N (BE 399.2 eV) as expected while, in contrast, the main N-species in the other 2 materials SiOAc-N2 and SiOAc-N1 was amide-N (BE 399.9—400.0 eV) [54]. This observation was also consistent with the appearances of amide-C (O=C—N) at 287.8—288.2 eV in the C1s spectra (Fig. 4c) and amide-O (O=C—N) at 531.0—531.4 eV in the O1s spectra (Fig. 4d) [54]. Table S3 summarizes our assignments for high-resolution XPS profiles of 4 representative hybrid materials.

Table 2
Nitrogen contents of 4 representative hybrid materials synthesized under optimum conditions (toluene, 180 °C) from the ester elimination route.

Material	SiOAc-N1	SiOAc-N2	SiOAc-N3-Me	SiOAc-N3
[a] **Calc. N (wt.%)**	7.21	4.09	4.37	2.86
[b] **Exp. N (wt.%)**	6.99	4.00	4.34	2.80

[a] Calculated from calc. Si contents (Table S2) and theoretical ratios Si/N of representative hybrid xerogels (Equations (1)—4).
[b] Obtained from Organic Elemental Analysis (CHNS).

The FT-IR spectra agreed well with the conclusions based on XPS spectroscopy. The FT-IR spectrum of SiOAc-N1 (Fig. 5, black) clearly confirmed the presence of secondary amide group with 4 typical bands: N-H stretch (3273 cm^{-1}), overtone of N-H bend (3085 cm^{-1}), C=O stretch (1633 cm^{-1}), and N-H bend (1551 cm^{-1}) [55] while the one of SiOAc-N2 (Fig. 5, red) confirmed the presence of tertiary amide group via the only C=O stretch band at 1625 cm^{-1}. The presence of tertiary amine groups in SiOAc-N3 and SiOAc-N3-Me was also confirmed by their FT-IR spectra (Fig. 5, blue and green, respectively) via the typical band at 2790—2802 cm^{-1} representing for C-H stretch of methyl/-methylene groups next to N in tertiary amine [30,31,56]. With results obtained from XPS and FT-IR, we conclude that only tertiary amine precursors (N3 or N3-Me) could co-polymerize with $Si(OAc)_4$ to form hybrid amine-silica materials under our non-hydrolytic sol-gel conditions while primary (N1) and secondary (N2) amine precursors formed hybrid secondary and tertiary amide-silica materials, respectively due to in-situ reactions between primary/secondary amine sites and co-product methyl acetate and/or $Si(OAc)_4$ precursor [27,46].

In agreement with XPS results, the STEM-EDS analysis of a selected hybrid material (SiOAc-N3-Me) showed the appearance of 4 elements (Si, N, C, and O) in its elemental composition. Most importantly, the STEM-EDS elemental mapping (scale bar 50 nm) also revealed a uniform distribution of these 4 elements with no single clusters (Fig. S8).

The FT-IR spectra (Fig. 5) also reveal that SiOAc-N3 and SiOAc-N3-Me contained unreacted acetoxy groups in their structure (C=O stretch at 1740—1742 cm^{-1}) while the other 2 materials SiOAc-N2 and SiOAc-N1 did not contain them. This observation also agreed with the weak signal of ester-C (O=C—O) at 288.7—289.1 eV in the high-resolution C1s spectra (Fig. 4c), the weak signal of ester-O (O=C—O) at 533.8—533.9 eV in the high-resolution O1s spectra (Fig. 4d), and the presence of unreacted methoxy and acetoxy groups in the solid-state ^{13}C CP MAS NMR spectra (Fig. 2) of SiOAc-N3 and SiOAc-N3-Me [54]. Since the silica and amine precursors were mixed with an equal number of acetoxy and methoxy functional groups at the beginning and the non-hydrolytic sol-gel reactions followed the ester elimination route to form methyl acetate as a volatile co-product together with hybrid gels, we assume that the more unreacted methoxy groups appeared in hybrid materials, the more unreacted acetoxy groups remained as well. Based on results from XPS and FT-IR as well as the absence of unreacted methoxy groups in the ^{13}C CP MAS NMR spectra (Fig. 2) of SiOAc-N1 and SiOAc-N2 materials, we could also conclude that the peaks at 174.0 & 171.5 ppm were not assigned to ester-C (O=C—O) but amide-C (O=C—N) instead in the ^{13}C CP MAS NMR spectra (Fig. 2) of SiOAc-N1 and SiOAc-N2 materials, respectively. The absence of unreacted methoxy and acetoxy groups of SiOAc-N1 and SiOAc-N2 materials could be due to higher degrees of co-polymerization compared to SiOAc-N3 and SiOAc-N3-Me materials and/or the in-situ formation of amide sites (confirmed by IR and XPS spectroscopy) leading to MeOH (observed by GC-MS) and/or ≡ SiOH formation under synthetic conditions. However, it should be noted that the FT-IR spectra (Fig. 5) showed no significant bands in the range 950—850 cm^{-1} (i.e., absorption band characteristic for Si—OH stretching vibration [57]), indicating insignificant appearance of silanol groups (Si—OH) in our hybrid materials compared to ones prepared via hydrolytic sol-gel method [30,31,56].

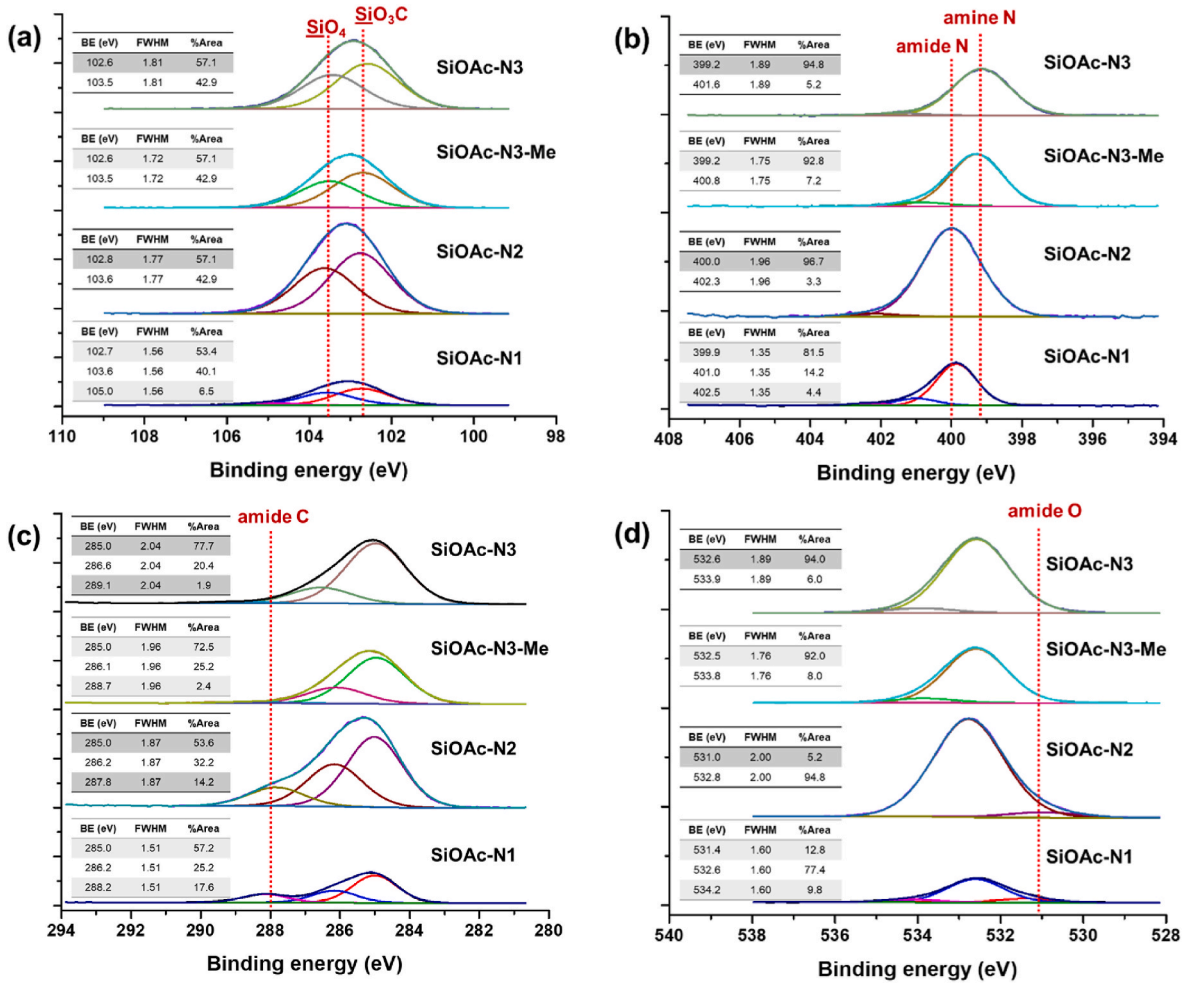

Fig. 4. High-resolution **(a)** Si2p, **(b)** N1s, **(c)** C1s, and **(d)** O1s XPS spectra of 4 representative hybrid materials synthesized under optimum conditions (toluene, 180 °C) from the ester elimination route. A minor component at 105.0 eV in Fig. 4a corresponds to SiO_4 and $CSiO_3$ moieties in hydrogen bonding (Table S3) [52].

3.3. *Ester elimination route: CO_2 adsorption on hybrid materials*

Fig. S9—12 illustrate CO_2 adsorption isotherms of 4 representative hybrid xerogels and their corresponding Freundlich–Langmuir (*aka* Sips) model fittings ($R^2 = 0.99996–1.00000$) at 3 different temperatures (0, 15, and 25 °C) [58,59]. Fig. S13 illustrates changes of the isosteric enthalpy of CO_2 adsorption (ΔH_{CO2_ads}) during the adsorption process obtained by Clausius–Clapeyron approach via Sips fit (i.e., Freundlich-Langmuir model) of CO_2 adsorption isotherms [58,59]. Table 3 summarizes main results obtained from these isotherms including the CO_2 uptake at 1 bar of CO_2 and the isosteric heat of CO_2 adsorption ($Q_{st} = -\Delta H_{CO2\_ads}$) at near-zero coverage. As expected, with N sites in the form of amide or tertiary amine and lack of other sites for CO_2 chemisorption, the Q_{st} values of hybrid materials were found in the range of 15–33 kJ mol^{-1}, representing mainly CO_2 physisorption ($Q_{st} <$ 50 kJ mol^{-1}) [60]. The comparable Q_{st} values (~25–27 kJ mol^{-1}) of SiOAc-N3 and SiOAc-N3-Me materials could be due to the similarities in specific surface area (761–776 $m^2\ g^{-1}$) and surface functional groups (e.g., tertiary amine, acetoxy, methoxy). Meanwhile, with slightly lower specific surface area (624 $m^2\ g^{-1}$), the highest Q_{st} value (33.23 kJ mol^{-1}) of SiOAc-N2 could be due to the presence of surface functional groups with higher polarities (e.g., tertiary amide, silanol). In contrast, the lowest Q_{st} value (14.54 kJ mol^{-1}) of SiOAc-N1 could be due to its non-porosity (<10 $m^2\ g^{-1}$) and the dissolution of CO_2 into the material matrix rather than only interactions on the material surface [61]. Basically, the heat of CO_2 absorption into dense rubbery matrices ($Q = -\Delta H$) includes 2 contributions: the heat of binding energy of CO_2 in matrix ($Q_1 > 0$) and the heat of reorganization ($Q_2 < 0$) [62]. Specifically, the Q_{st} value of SiOAc-N1 is quite comparable to the heat of CO_2 dissolution into the polymeric matrix of poly(methyl propyl siloxane) with $Q =$ 14.69 kJ mol^{-1} [63].

Overall, the CO_2 uptake of hybrid materials decreased when increasing sorption temperature from 0 to 25 °C and did not reach a plateau at 1 bar of CO_2 (Fig. S9—12), indicating that the CO_2 uptake could be improved further at higher CO_2 pressure. The CO_2 uptake (mmol/g) at same conditions is in the order of SiOAc-N2 > SiOAc-N3 ~ SiOAc-N3-Me > SiOAc-N1 (Table 3). This order also agrees with the differences in porosity and surface functional groups of materials already mentioned above when comparing Q_{st} values. It should be noted that in carbon dioxide physisorption, CO_2 molecules are attracted by solid adsorbent mainly via van-der-Waals forces as well as electrostatic interactions between CO_2 molecules and polar sites on adsorbent surface thanks to having CO_2 quadrupole moment [64]. Although the similarities in specific surface area (761–776 $m^2\ g^{-1}$) and surface functional groups (e.g., tertiary amine, acetoxy, methoxy) of 2 materials SiOAc-N3 and SiOAc-N3-Me, the CO_2 uptake per nitrogen site (mmol CO_2/mmol N) in SiOAc-N3 is higher than SiOAc-N3-Me (e.g., 0.200 vs 0.125 mmol CO_2/mmol N at 25 °C, respectively, Table 3), indicating minor contribution of tertiary amine for CO_2 uptake at 1 bar of CO_2. Specifically, comparing to SiOAc-N3 (similar specific surface area), higher content of tertiary amine (higher N content) in SiOAc-N3-Me (4.34 vs 2.80 wt% N, respectively, Table 4) did not lead to higher CO_2 uptake (mmol/g) at 1 bar of CO_2 but lower CO_2 uptake per nitrogen site (mmol CO_2/mmol N). The hybrid material SiOAc-N2 derived from NHSG also showed a

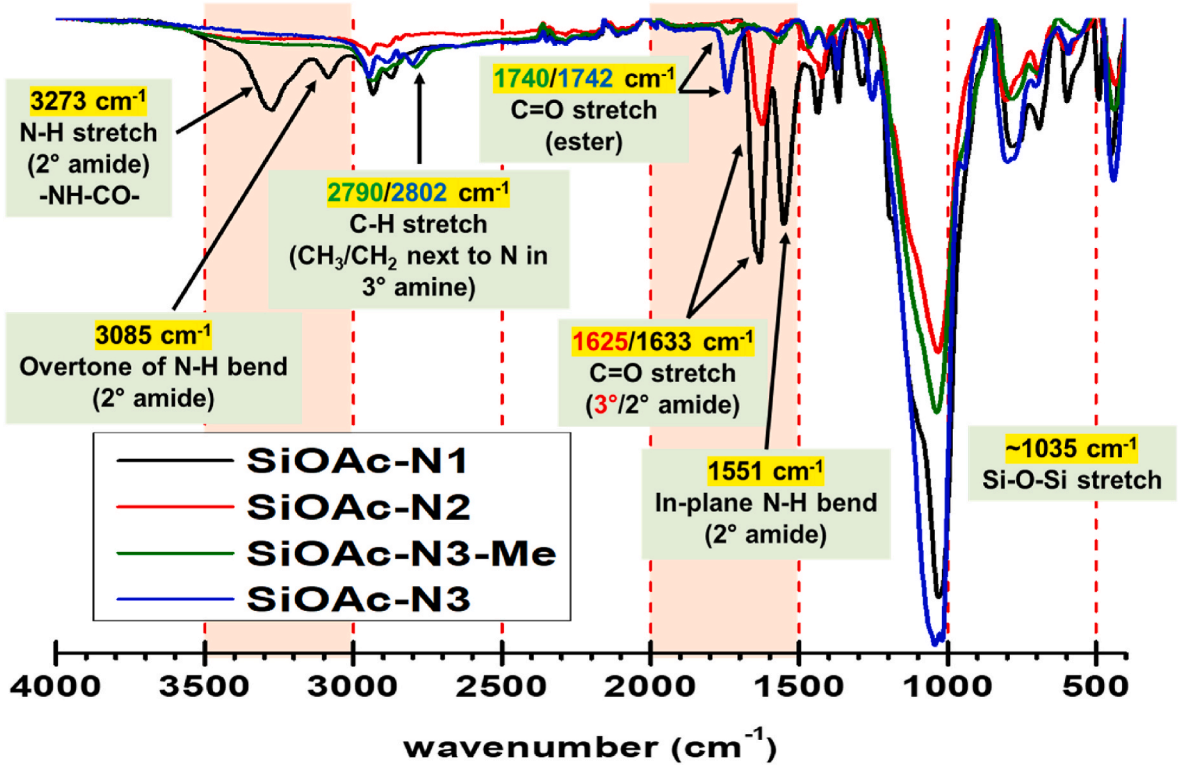

Fig. 5. FT-IR spectra of 4 representative hybrid materials synthesized under optimum conditions (toluene, 180 °C) from the ester elimination route.

Table 3
CO_2 uptakes and isosteric heat values of CO_2 adsorption of 4 representative hybrid xerogels synthesized under optimum conditions (toluene, 180 °C) from the ester elimination route.

Material	CO_2 uptake at 1 bar of CO_2 [a] (mmol/g)			Q_{st} at near-zero coverage (kJ mol^{-1})
	0 °C	15 °C	25 °C	
SiOAc-N1	0.174 (0.035)	0.136 (0.027)	0.092 (0.018)	14.54 ± 5.41
SiOAc-N2	1.014 (0.355)	0.742 (0.260)	0.584 (0.204)	33.23 ± 0.05
SiOAc-N3-Me	0.674 (0.218)	0.482 (0.156)	0.386 (0.125)	24.67 ± 1.62
SiOAc-N3	0.731 (0.366)	0.543 (0.272)	0.399 (0.200)	26.59 ± 3.15

[a] Numbers in parenthesis are presented in mmol CO_2/mmol N. The N contents are obtained from Organic Elemental Analysis (CHNS).

comparable or even better CO_2 sorption capacity compared to similar hybrid materials derived from HSG using the same amine precursor (N2) probably thanks to a higher specific surface area of SiOAc-N2 [35,65].

3.4. Alkyl halide elimination route

In this route, $SiCl_4$ was used as a silica precursor together with 4 amine precursors (N1/N2/N3-Me/N3) containing trimethoxysilyl groups to synthesis of hybrid materials (Equation (1)—4). The silica and amine precursors were mixed with an equal number of chloride and methoxy functional groups in an aprotic solvent. The presence of methyl chloride as a volatile product in all synthesis experiments was confirmed by GC-MS analysis of residue solvents after the non-hydrolytic sol-gel (NHSG) synthesis.

Table 4 summarizes the textural properties of hybrid materials synthesized from the alkyl halide elimination route under different synthetic conditions (amine precursor, aprotic solvent). Like the ester elimination route, materials derived from the terminal amine precursor (N1) were also low/non-porous (2—14 m^2 g^{-1}) in the alkyl halide elimination route. In contrast, even though toluene (TOL) was the optimal solvent to prepare highly porous materials with preserved organic moieties coming from bridging amine precursors in the ester elimination route (Table 1, Fig. 2 and S5), the material synthesized from $SiCl_4$ and N2 precursor in TOL was non-porous (<10 m^2 g^{-1}). The

Table 4
Textural properties of hybrid amine-silica xerogels obtained from the alkyl halide elimination route ($SiCl_4$ as a silica precursor) under different conditions.

Gel	Amine precursor	Aprotic solvent	Temp. (°C)	S_{BET} (m^2 g^{-1})	[a]V_{total} (cm^3 g^{-1})	[b]$V_{micro}/V_{tot.}$ (%)	[c]PS_{DFT} (nm)	[d]$PS_{aver.}$ (nm)
1	N1	TOL	180	<10	n.d.	n.d.	n.d.	n.d.
2		DCM	180	14	0.05	0	16.1	13.4
3	N2	TOL	180	<10	n.d.	n.d.	n.d.	n.d.
4		DCM	180	351	0.65	5.2	2.6	7.4
5	N3-Me	DCM	180	300	0.50	12.0	2.6	6.7
6	N3	DCM	180	575	1.31	4.2	2.6	9.1

n.d. = not determined.
[a] Estimated at $p/p_o = 0.97$.
[b] Based on t-plot analysis (Fig. S16).
[c] The maximum value of the pore size distribution curve (NLDFT, ads, cyl. pore model).
[d] $4V_{total}/S_{BET}$.

sample derived from bridging amine precursor N2 and $SiCl_4$ in dichloromethane (DCM) showed high specific surface area (351 $m^2\ g^{-1}$) and high total pore volume (0.65 $cm^3\ g^{-1}$). Accordingly, reactions between $SiCl_4$ and N3 and N3-Me were performed in DCM and exhibited high S_{BET} (300—575 $m^2\ g^{-1}$), high V_{total} (0.50—1.31 $cm^3\ g^{-1}$), and pore size distribution in mesopore range (Table 4).

The solid-state ^{13}C CP TOSS MAS NMR spectra revealed the complicated organic structures of the hybrid materials obtained from the alkyl halide elimination route either in TOL or DCM (Fig. S14), indicating a negative effect of using $SiCl_4$ as a silica precursor on the structural integrity of organic moieties after NHSG synthesis. This observation could be mainly due to in-situ reactions between amine sites and co-product CH_3Cl under synthetic conditions to form a complicated mixture including quaternary ammonium chloride salts as well as their corresponding thermal decomposition products via the reverse Menschutkin and/or Hofmann reactions (described in detail in section 3.6 Recyclability studies and spent catalysts characterization with [4-(chloromethyl)-1,3-dioxolan-2-one] as the model quaternization agent) [49–51]. Noteworthy, the quaternary (alkyl)ammonium halides are often used as co-catalysts for CO_2 cycloaddition reactions with iodides and bromides being highly preferred [66,67]. Therefore, application of $SiBr_4$ or SiI_4 in alkyl halide elimination might lead to catalytically interesting materials.

The survey scan XPS spectra (not shown) revealed the appearance of 5 elements (Si, N, C, O, and Cl) on the surfaces of representative hybrid materials prepared in DCM or TOL by the alkyl halide elimination route. The high-resolution N1s XPS spectra (Fig. 6a) showed 2 major peaks at binding energies (BE) ~399.5 and ~401.9 eV corresponding to amine-N (N_A) and quaternary ammonium N (N_{QA}), respectively [54]. The N_{QA}/N_A ratio decreased from 8.3 to 1.8 when the steric hindrance on N site increased (i.e., from N1 to N3 precursor), indicating the decrease in degree of quaternization of amine sites (Fig. 6a). Meanwhile, the high-resolution Cl2p XPS spectra (Fig. 6b) revealed the presence of Cl^- anions from quaternary ammonium salts at BE~197.7 eV as well as C—Cl at BE~200.6 eV in the Cl2p3/2 spectra [54]. The appearance of C—Cl in the structure could be due to side reactions between amine sites and DCM under synthetic conditions as already observed in the ester elimination route (Fig. S15) and/or thermal decomposition products of quaternary ammonium chloride salts (see discussion in section 3.6 Recyclability studies and spent catalysts characterization) [48,49].

3.5. Investigation of synthesized hybrid materials as heterogeneous catalysts for the CO_2 cycloaddition to epoxides

In order to investigate the catalytic potential of synthesized hybrid amine-silica materials as alternative metal- and halogen-free heterogeneous catalysts for direct conversion of CO_2 to cyclic carbonates under solvent-free and co-catalyst-free conditions, screening catalytic tests were performed in a custom-made high-pressure batch reactor (Fig. S17) using near-stoichiometric amount of CO_2 (~14 mmol or 10 bar of initial CO_2 pressure) and epichlorohydrin (10 mmol) at 120 °C for 1 h. Table 5 summarizes the main catalytic results from selected catalysts synthesized using non-hydrolytic sol-gel (NHSG) method via the ester elimination route in TOL at 180 °C for 4 days (SiOAc). Increasing the initial CO_2 pressure from 10 to 15 bar (entries 9 and 10) just improved slightly the epoxide conversion, indicating that 10 bar of initial CO_2 pressure is the optimal pressure for our reaction conditions.

For the sake of comparison of catalytic activity, selected catalysts synthesized using non-hydrolytic sol-gel (NHSG) method via the alkyl halide elimination in DCM at 180 °C for 4 days (SiCl) were also tested at similar catalytic reaction conditions (50 mg of catalyst, 10 bar of CO_2, 10 mmol of epichlorohydrin, 120 °C, 1 h). Results are summarized in Table S4 even though the chemical structure of these materials (SiCl) was not well-defined due to their complicated organic structures (Fig. S14). Overall, all synthesized hybrid materials were active with high selectivity to cyclic carbonate (>99 %) and low-to-high conversion of epichlorohydrin (11—86 %) under investigated conditions. Commercial porous silica showed no activity (entry 1), indicating the catalytic role of N sites in hybrid materials for the CO_2 cycloaddition to epichlorohydrin. The materials prepared by alkyl halide elimination exhibit higher epichlorohydrin conversions than corresponding samples prepared by ester elimination except for amine-functionalized silica prepared from N3-Me (Table 5 and Table S4). On one hand, the materials prepared from $SiCl_4$ contain quaternary alkylammonium chloride sites that might be beneficial for CO_2 cycloaddition. On the other hand, poorly defined moieties coming from the decomposition of quaternary ammonium sites might be incorporated in SiCl materials as well. Therefore, it is not possible to explain unambiguously the differences between SiCl and SiOAc samples.

Among hybrid materials prepared by ester elimination, SiOAc-N3-Me showed the highest catalytic activity (TOF = 358 h^{-1}). Most importantly, the order of catalytic activity in decreasing order of turnover frequency (TOF) was SiOAc-N3-Me > SiOAc-N3 ≫ SiOAc-N2 > SiOAc-N1 (entries 2–4, 8), indicating that tertiary amine-N sites (SiOAc-N3-Me and SiOAc-N3) were much more active for the reaction than

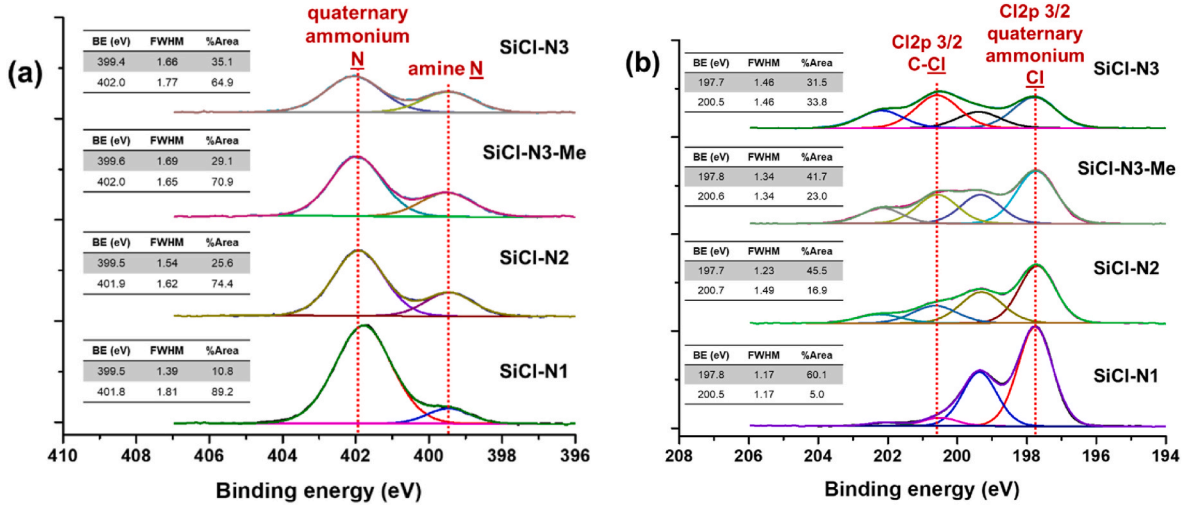

Fig. 6. High-resolution **(a)** N1s and **(b)** Cl2p XPS spectra of 4 representative hybrid materials synthesized in DCM from the alkyl halide elimination route.

Table 5
Summary of batch catalytic experiments conducted on the cycloaddition reaction of epoxides and CO_2.

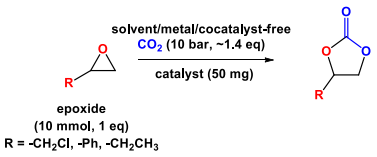

entry	catalyst	epoxide	temp. (°C)	time (h)	conv.[a] (%)	sel.[a] (%)	$k_{ini.}$[b] (h^{-1})	TOF[c] (h^{-1})
1	Commercial SiO_2 (Aerosil 300)	epichlorohydrin	120	1	0	–	–	–
2	SiOAc-N1	epichlorohydrin	120	1	11	>99	0.12	4.7
3	SiOAc-N2	epichlorohydrin	120	1	14	>99	0.15	10.5
4	SiOAc-N3	epichlorohydrin	120	1	56	>99	1.81	181
5			100	1	34	>99	0.42	41.6
6			90	1	20	>99	0.22	22.3
7			80	1	10	>99	0.11	10.5
8	SiOAc-N3-Me	epichlorohydrin	120	1	86	>99	5.54	358
9			100	1	52	>99	0.89	57.6
10[d]			100	1	55	>99	n.d.	n.d.
11			90	1	38	>99	0.51	33.0
12			80	1	25	>99	0.29	18.6
13		styrene oxide	120	14	51	>99	n.d.	n.d.
14			140	14	97	>99	n.d.	n.d.
15		1,2-butylene oxide	120	14	55	>99	n.d.	n.d.
16	Tripropylamine (14 mg, 0.098 mmol)[e]	epichlorohydrin	100	1	42	>99[g]	0.42	43.0
17			90	1	16	>99[g]	0.17	17.8
18			80	1	7	>99[g]	0.07	7.4
19	Methyldipropylamine (17 mg, 0.148 mmol)[f]	epichlorohydrin	100	1	80	>99[g]	1.95	132
20			90	1	62	>99[g]	0.65	43.9
21			80	1	32	>99[g]	0.39	26.1

n.d. = not determined.
[a] Based on ^{1}H NMR and GC-MS analysis.
[b] Calculated based on the initial rate of epichlorohydrin conversion.
[c] TOF $= \frac{k_{ini.} * n_{epoxide}}{n_{N\ sites}}$ with $n_{N\text{-}sites}$ based on Organic Elemental Analysis.
[d] Initial pressure of CO_2 = 15 bar.
[e] Organic structure analog of SiOAc-N3, comparable N content based on Organic Elemental Analysis.
[f] Organic structure analog of SiOAc-N3-Me, comparable N content based on Organic Elemental Analysis.
[g] Excluding by-products derived from reactions between amines and epichlorohydrin/cyclic carbonate due to difficulty in distinguishing by NMR.

amide-N sites (SiOAc-N2 and SiOAc-N1). This observation also agrees with the use of tertiary amines as highly efficient organocatalysts for CO_2 fixations [17]. While catalytic activity appear to strongly depend on the active sites (tertiary amine-N vs. amide N), the porosity does not seem to play a decisive role: Non-porous SiOAc-N1 exhibited a similar epichlorohydrin conversion as highly porous SiOAc-N2.

The catalyst SiOAc-N3-Me was also active for the CO_2 cycloaddition to different epoxides other than epichlorohydrin such as styrene oxide and 1,2-butylene oxide (entries 13–15). Among the 3 epoxides, epichlorohydrin is the most reactive one thanks to the presence of an electron-withdrawing chloromethyl group (—CH_2Cl) that activated the epoxide ring, rendering it more susceptible for nucleophilic attack by tertiary amine-N sites and/or activated CO_2 [17]. The lowest reactivity of styrene oxide could be due to the steric effect of the phenyl group next to the epoxide ring. This observed trend of epoxide reactivity for mesoporous tertiary amine-silica hybrid SiOAc-N3-Me catalyst is also in agreement with mesoporous melamine-formaldehyde resin MMFR catalyst, where epoxide reactivity decreased in the same order (i.e., epichlorohydrin ≫ 1,2-butylene oxide > styrene oxide) [23].

Reported mesoporous amine-silica hybrid catalysts in the literature for the synthesis of cyclic carbonates from CO_2 in batch reactor under solvent-free condition are also summarized and compared with this work in Table S5. More specifically, although the N contents of our catalysts are lower than the N contents of Si-Imid and SiO_2-His materials, the catalytic performances of our catalysts are still comparable or even higher [27,28], indicating that aliphatic tertiary amine sites are more efficient than imidazole or histidine in this case. Significantly higher catalytic activities have been reported only for catalysts containing metals and in the presence of co-catalysts: 16 wt% APTES@ZrO_2-MCM-41 and SBA-15/N-Au showed more than 90 % of cyclic carbonate yield at 80 °C [66,67]. Finally, with epichlorohydrin as an epoxide substrate, our catalysts showed higher catalytic performance than most of the reported mesoporous amine-silica (with/without metal) catalysts except for PT@SBA-16, while it is not the case with styrene oxide or 1,2-butylene oxide as an epoxide substrate [27–29,68]. This observation is also true when comparing our catalysts with the reported catalyst B-SBA-15-NH_2 in the presence of co-catalyst KI [69]. The observation could be explained by in-situ reactions of our catalysts with epichlorohydrin and/or [4-(chloromethyl)-1,3-dioxolan-2-one] to create quaternary ammonium chloride as another active form for the synthesis of cyclic carbonate (see mechanism below in section 3.6 Recyclability studies and spent catalysts characterization) [48–51].

In order to understand better the catalytic activity of tertiary amine-N sites in mesoporous tertiary amine-silica hybrids (SiOAc-N3-Me and SiOAc-N3), the organic structure analogues (methyldipropylamine (MDPA) and tripropylamine (TPA)) were also tested as homogeneous catalysts at similar catalytic reaction conditions (entries 16–21) and compared in terms of turnover frequency (TOF), apparent activation energy (E_a) and pre-exponential factor (A) (Table 5, Fig. 7). The mass of homogeneous catalysts MDPA and TPA was taken to have a comparable N content in 50 mg of heterogeneous catalysts SiOAc-N3-Me (0.155 mmol of N) and SiOAc-N3 (0.100 mmol of N), respectively, based on organic elemental analysis. The temperature range for comparison was chosen from 80 to 100 °C to avoid very slow or fast initial rate of epichlorohydrin conversion under our reaction conditions. The catalytic reaction was assumed to follow pseudo-first-order kinetics based on

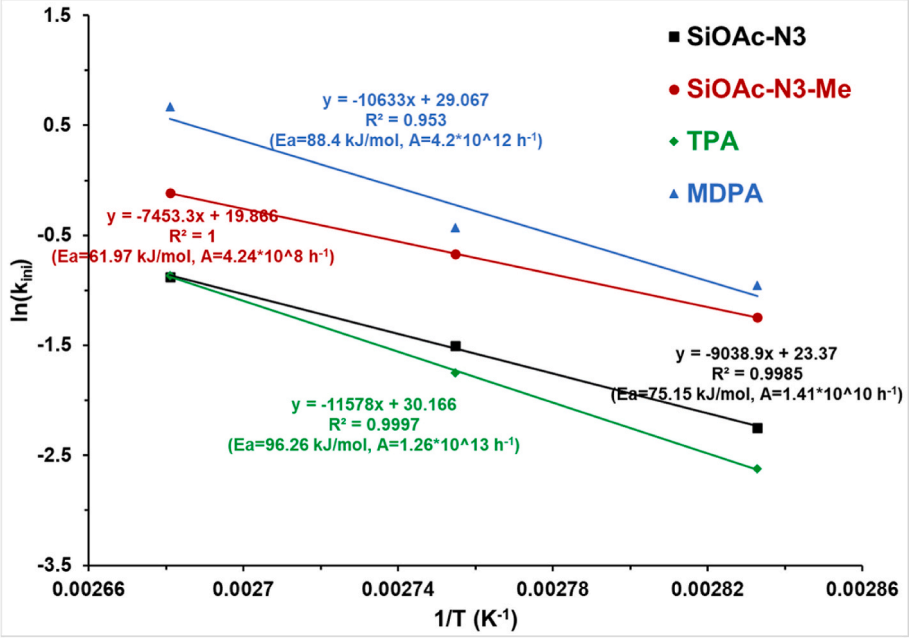

Fig. 7. Arrhenius-like plots ($\ln(k_{ini})$ vs. 1/T) for mesoporous tertiary amine-silica hybrids (SiOAc-N3 and SiOAc-N3-Me) as heterogeneous catalysts and their organic structure analogues (TPA and MDPA) as homogeneous catalysts for epichlorohydrin conversion at 80–100 °C (cyclic carbonate selectivity in all cases >99 %). The Arrhenius-like plots with high R^2 (0.95–1.00) justify the hypothesis of a pseudo 1st order reaction.

epichlorohydrin concentration. Apparent activation energy (E_a) and pre-exponential factor (A) were calculated from the Arrhenius-like plots of $\ln(k_{ini})$ vs. 1/T, where k_{ini} refers to rate constant calculated based on the initial rate of epichlorohydrin conversion (Fig. 7) [23].

Overall, the order of catalytic activity in decreasing order of turnover frequency (TOF) was MDPA > SiOAc-N3-Me > SiOAc-N3 ~ TPA, indicating that tertiary amine-N sites with one methyl and two propyl groups are more active than ones with three propyl groups. These observed results agree with a higher degree of steric hindrance of three propyl groups surrounding tertiary amine-N sites, hindering the nucleophilic attack of tertiary amine-N sites on epoxide ring and/or CO_2. The higher TOF values of MDPA compared to ones of SiOAc-N3-Me (e.g., 26.1 vs. 18.6 h^{-1}, respectively, at 80 °C) can be expected because the number of accessible tertiary amine-N sites on the surface of SiOAc-N3-Me is likely to be lower than the total N content in SiOAc-N3-Me calculated from the organic elemental analysis. However, this trend was not observed in the case of TPA and its solid counterpart SiOAc-N3. The TOF value of TPA was only slightly higher than one of SiOAc-N3 at 100 °C (43.0 vs. 41.6 h^{-1}, respectively) but lower at 80 and 90 °C, indicating tertiary amine-N sites of heterogeneous catalyst SiOAc-N3 are more efficient for the reaction than ones of homogeneous catalyst TPA. These results also agree with lower apparent activation energy derived from the Arrhenius-like plots of $\ln(k_{ini})$ vs. 1/T (Fig. 7) of SiOAc-N3 compared to TPA in the temperature range of 80—100 °C (75.15 vs. 96.26 kJ mol^{-1}, respectively). Interestingly, the apparent activation energy of the heterogeneous catalyst SiOAc-N3-Me is also lower than the analogue homogeneous catalyst MDPA (61.97 vs. 88.4 kJ mol^{-1}, respectively) (Fig. 7), indicating that tertiary amine-N sites of heterogeneous catalyst SiOAc-N3-Me are also more efficient for the reaction than ones of homogeneous catalyst MDPA. It was reported that, in some cases, the silica-supported catalysts showed a higher catalytic activity than the homogeneous counterparts thanks to a synergistic effect between surface silanol groups and active sites [70–74]. Since no evidence of silanol groups of SiOAc-N3-Me and SiOAc-N3 was obtained from FTIR (Fig. 5), it was not clear what are the reasons for the observed results. Possible explanation might originate from the in-situ changes of both homogeneous tertiary amines and the amine-functionalized silicas during catalytic experiments (Figs. S18 and S19, see section 3.6 Recyclability studies and spent catalysts characterization).

3.6. Recyclability studies and spent catalysts characterization

In order to investigate the operational stability of the catalyst SiOAc-N3-Me, reusability studies were conducted in a custom-made high-pressure batch reactor under selected reaction conditions (120 °C, 10 bar of initial CO_2 pressure, 1 h) using epichlorohydrin as a reactant. Fig. 8a showed that although the catalytic activity of the catalyst SiOAc-N3-Me reduced after the 1st recycle, the activity loss was less significant after the 2nd and 3rd recycles and almost negligible after the 4th recycle. Characterization of spent catalysts by means of FT-IR (Fig. 8b) disclosed the presence of strongly adsorbed cyclic carbonate product (1793 cm^{-1}) [23]. This observation also agrees with the decrease in specific surface area and total pore volume of the 1st spent catalyst compared to the fresh one (Fig. S20). In addition, XPS analysis of spent catalysts (Fig. S21) also showed the appearance of adsorbed cyclic carbonate product derived from epichlorohydrin in the C1s branch (O—CO—O peak at 290.7 eV), in the O1s branch (O—CO—O peak at 534.1 eV) and especially in the Cl2p branch (Cl^- anion peak from chloride salt or chemisorption of cyclic carbonate product at 197.5—197.6 eV as well as C—Cl peak from physisorption of cyclic carbonate product at 200.4—200.5 eV) [23,51]. The presence of quaternary ammonium peak at 402.3—402.4 eV in the N1s branch (Fig. S21) of spent catalysts [54] also confirms the presence of chemisorbed cyclic carbonate via quaternization of tertiary amine group of the solid catalyst with chloromethyl group (—CH_2Cl) of cyclic carbonate product [50,51].

Table 6 summarizes the elemental composition of C, O, Cl, and N-species (normalized based on Si (at.%)) on the surface of fresh and spent catalysts (XPS). Overall, the C/Si and O/Si ratios increased from fresh catalyst to 1st spent and 4th spent catalysts, indicating the accumulation of chemi/physisorbed cyclic carbonate product [4-(chloromethyl)-1,3-dioxolan-2-one] on the catalyst surface. The content of Cl^-, C—Cl, amine-N, and ammonium-N normalized per Si confirm the quaternization of amine sites (SiOAc-N3-Me, both 1st and 4th spent) [50,51]. The decrease in Cl^- and ammonium-N content in 4th spent catalyst compared to 1st spent catalyst could be due to thermal decomposition of quaternary ammonium chloride sites via the reverse Menschutkin

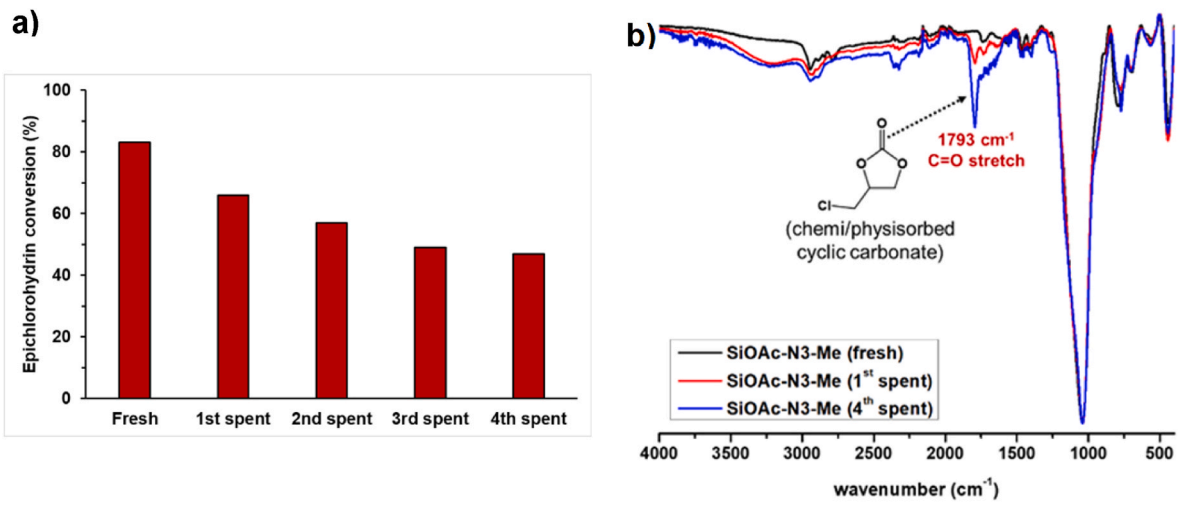

Fig. 8. **(a)** Reuse tests of the catalyst SiOAc-N3-Me under reaction conditions: 50 mg of catalyst, 10 mmol of epichlorohydrin, 10 bar of initial CO_2 pressure, 120 °C, 1 h; **(b)** FT-IR spectra of fresh and spent catalysts.

Table 6
XPS composition of surface of fresh and spent catalysts.

material	total Cl/Si		total N/Si		total C/Si	total O/Si
	anion Cl/Si	C—Cl/Si	amine N/Si	ammonium N/Si[a]		
SiOAc-N3-Me (fresh)	0.00	0.00	0.28	0.03	2.49	1.90
SiOAc-N3-Me (1st spent)	0.13	0.07	0.15	0.15	3.38	2.34
SiOAc-N3-Me (4th spent)	0.08	0.09	0.17	0.11	4.04	2.83

[a] protonated/hydrogen bonded amine also has similar binding energy to quaternary ammonium.

and/or Hofmann reactions during reusability studies [49].

The ^{13}C CP MAS NMR spectrum of the 1st spent catalyst (Fig. S22a) showed broaden peaks in the range of 30—85 ppm, indicating the presence of adsorbed cyclic carbonate product. In addition, the appearance of new peaks at 20 and 29 ppm could be due to chemisorbed cyclic carbonate and/or thermal decomposition products of chemisorbed cyclic carbonate. More specifically, the peak at 20 ppm (4 ppm lower than carbon#2 of SiOAc-N3-Me) could be assigned to carbon#2 of quaternary ammonium propyl silica while the peak at 29 ppm (5 ppm higher than carbon#2 of SiOAc-N3-Me) could be assigned to carbon#2 of 3-chloropropyl silica derived from the in-situ decomposition of the chemisorbed cyclic carbonate product via the reverse Menschutkin reaction (Fig. S22b). It should be noted that two quaternary ammonium iodides in Fig. S22b were used as arbitrary benchmarks for the chemisorbed cyclic carbonate (quaternary ammonium chloride derived from SiOAc-N3-Me).

Based on the experimental results, we proposed a possible way of chemisorption of cyclic carbonate [4-(chloromethyl)-1,3-dioxolan-2-

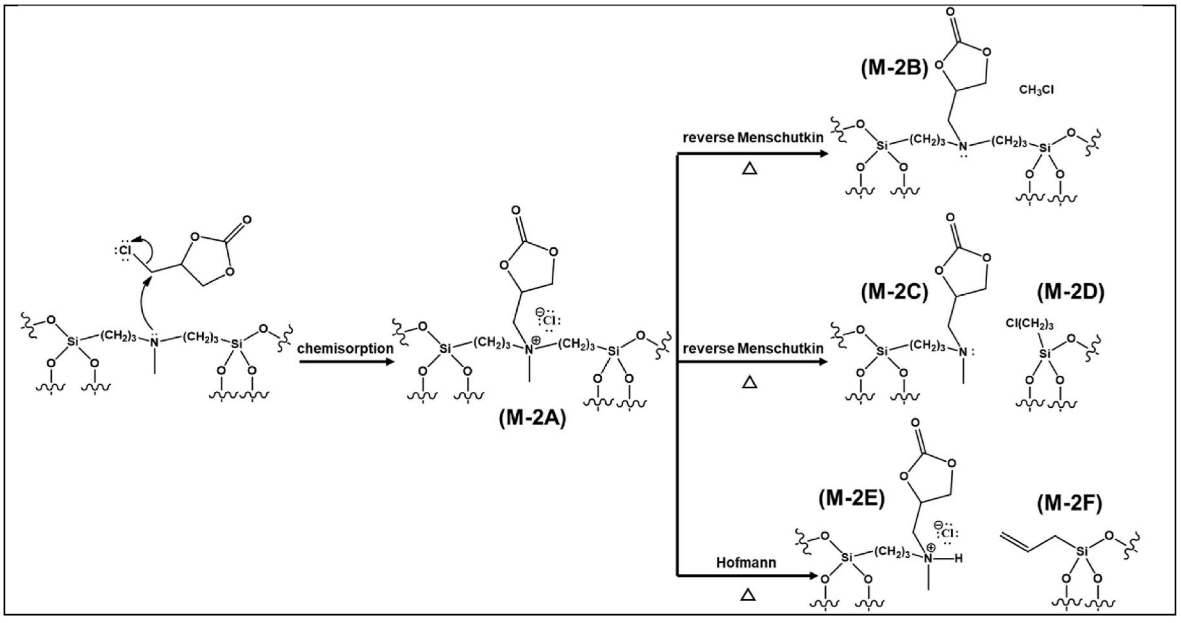

Scheme 1. A possible way of chemisorption of cyclic carbonate [4-(chloromethyl)-1,3-dioxolan-2-one] and suggested decomposition products via the reverse Menschutkin and Hofmann reactions.

one] via tertiary amine site quaternization (Scheme 1, M-2A) [50,51]. Moreover, some possible decomposition products were suggested via the reverse Menschutkin and Hofmann reactions (Scheme 1, M-2B−F) [49].

To sum up, a strong deactivation of our tertiary-amine-functionalized silica catalyst (SiOAc-N3-Me) upon recycling tests with epichlorohydrin as an epoxide reactant could be mainly due to strong chemi/physisorption of cyclic carbonate product on the catalyst surface, confirmed by FTIR, N_2 physisorption, XPS, and ^{13}C CPMAS NMR techniques. These strong adsorptions could block some active sites and increase the mass of spent catalysts, leading to fewer active sites per mass unit of spent catalysts. It should be mentioned that repeated quaternization and decomposition reactions (Scheme 1) may also lead to some leaching of active sites during recycling tests.

Noteworthy, a strong deactivation upon recycling was also observed for silica-based catalysts with grafted ammonium groups. The loss of catalytic activity was explained by both leaching of active species and polymerization of substrate (styrene oxide) on the catalyst's surface hence making the active sites inaccessible [74]. However, since the authors did not characterize their spent catalysts by FT-IR or XPS, it was not clear whether they could observe strong adsorption of styrene carbonate on their catalyst surface or not.

3.7. Plausible mechanism for the synthesis of cyclic carbonate from epichlorohydrin and CO_2

Analysis of ^1H NMR spectra of the reaction mixtures using epichlorohydrin (ECH) as an epoxide reactant and tertiary aliphatic amines as homogeneous catalysts (Figs. S18 and S19) showed that the intensity of original amine catalysts decreased while the intensity of unknown peaks increased during the initial stage of catalysis. These results indicate that amine catalysts could react with ECH and/or cyclic carbonate product to form other reactive intermediates, probably quaternary ammonium chlorides [50,51].

Similar to the homogeneous catalytic tests, analysis of XPS profiles of spent tertiary-amine-functionalized silica catalysts also showed the presence of quaternary ammonium chloride sites on the surface together with amines (Fig. S21).

Based on these experimental results, we proposed a plausible mechanism for the synthesis of cyclic carbonate from ECH and CO_2 using SiOAc-N3-Me as a heterogeneous catalyst in Scheme 2.

On the one hand, the reaction could be initiated by the formation of a reactive quaternary ammonium chloride intermediate (M-1A) on the surface of the catalyst, followed by the nucleophilic attack of chloride anion on the less substituted carbon atom of the epoxide ring leading to the formation of a zwitterionic species (M − 1B) (route 1).

On the other hand, since the SiOAc-N3-Me catalyst was also active with other epoxides such as 1,2-butylene oxide and styrene oxide for the synthesis of cyclic carbonates (Table 5) and XPS profiles of spent catalysts (after testing with ECH) still showed more than 50 % of amine-N in total N-species (Fig. S21, Table 6), we proposed the reaction could simultaneously follow route 2, where the nucleophilic attack of tertiary aliphatic amine on the less substituted carbon atom of the epoxide ring leads to the formation of the same zwitterionic species (M − 1B) like route 1 [17,19].

Then, the negatively charged oxygen atom of the intermediate M − 1B could further react with the electrophilic carbon of CO_2 under high pressure of CO_2 (10 bar) to form the intermediate M − 1C, followed by the intramolecular cyclization to produce the cyclic carbonate product and regenerate the tertiary-amine-functionalized silica catalyst.

4. Conclusions

Herein, we presented for the first time the non-hydrolytic sol-gel synthesis of amine-functionalized silicas. The ideal synthetic conditions include the application of silicon tetraacetate and bridging tertiary amine silanes as precursors, toluene as a solvent, and temperature between 160 and 180 °C. Neither template nor catalyst is necessary to obtain highly porous materials (up to 776 $m^2\,g^{-1}$ and 1.58 $cm^3\,g^{-1}$) with preserved and homogeneously dispersed amine moieties in one-step process. The application of silicon tetrachloride and/or dichloromethane as a solvent leads to the in-situ quaternization of amine sites and other side reactions; the use of primary and secondary amine silane precursors leads to the in-situ formation of secondary, and tertiary amide groups, respectively, in the application of silicon tetraacetate.

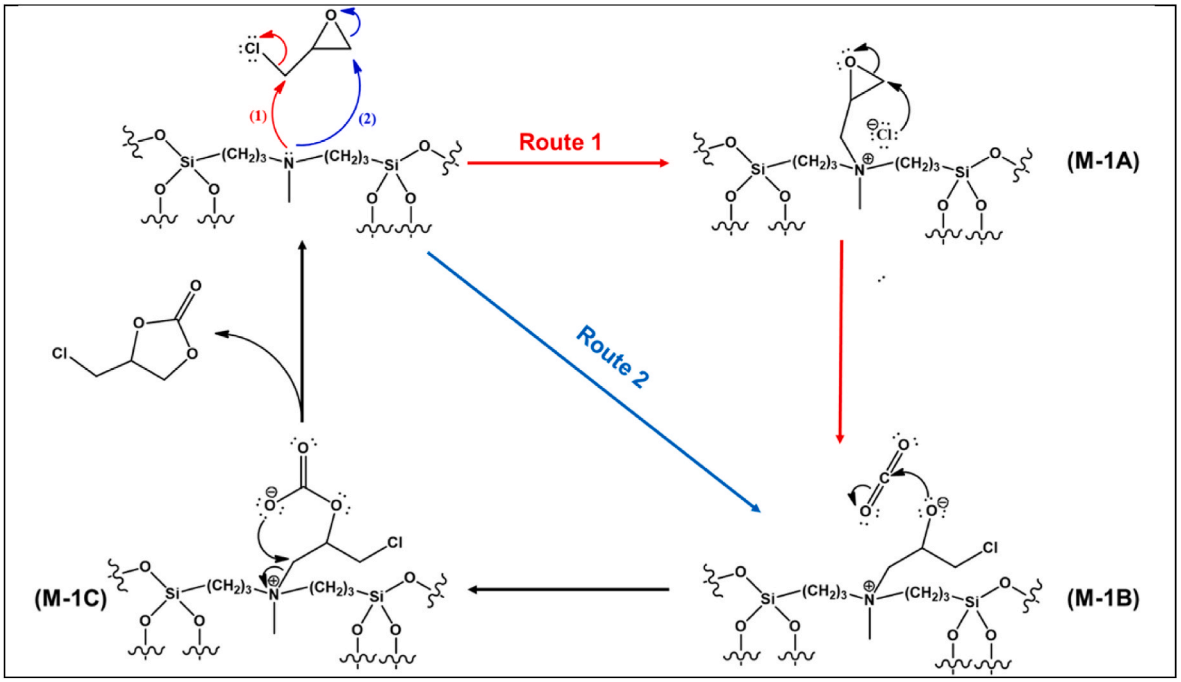

Scheme 2. Proposed mechanism for the synthesis of cyclic carbonate [4-(chloromethyl)-1,3-dioxolan-2-one] from epichlorohydrin and CO_2 using catalyst SiOAc-N3-Me. Please note the similarities between M-1A and M-2A intermediates (Schemes 1 and 2).

Both processes (described with the help of IR, MAS NMR, and XPS spectroscopy) lead to the unwanted changes to the amine sites.

The catalytic properties of synthesized materials were tested in CO_2 coupling with epichlorohydrin, styrene oxide, and 1,2-butylene oxide providing corresponding cyclic organic carbonates with high selectivity in all cases (>99 %). The highest catalytic activity was exhibited by a material synthesized with the use of bis[3-(trimethoxysilyl)propyl]-N-methylamine as the tertiary amine site source (**SiOAc-N3-Me**; 86 % epichlorohydrin conversion after 1 h at 120 °C and 10 bar CO_2). Interestingly, this catalyst showed a lower apparent activation energy in comparison to its homogeneous analogue, methyldipropylamine (62 vs. 88 kJ mol^{-1}), when converting epichlorohydrin to 4-(chloromethyl)-1,3-dioxolan-2-one (cyclic carbonate product). The application of epichlorohydrin as reaction substrate led to the in-situ quaternization of amine sites in the catalysts. Moreover, the 4-(chloromethyl)-1,3-dioxolan-2-one (or its derivatives) was present in the spent catalyst even after extensive washing. Both processes probably caused the decrease of catalytic activity upon catalyst's recycling. However, the catalytic activity stabilized at 57 % of the initial activity after the fourth catalytic cycle.

CRediT authorship contribution statement

Thai Q. Bui: Writing – review & editing, Writing – original draft, Visualization, Methodology, Investigation. **Tomas Pokorny:** Writing – review & editing, Investigation. **Petr Machac:** Writing – review & editing, Investigation. **Zdenek Moravec:** Writing – review & editing, Investigation. **Eva Domincova Bergerova:** Writing – review & editing, Investigation. **Ales Styskalik:** Writing – review & editing, Supervision, Project administration, Funding acquisition, Conceptualization.

Data availability

Data for this article are available at Zenodo at https://zenodo.org/records/12649427 (DOI = . 10.5281/zenodo.12636393).

Declaration of competing interest

The authors declare that they have no known competing financial interests or personal relationships that could have appeared to influence the work reported in this paper.

Acknowledgements

The financial support of Grant Agency of Masaryk University (GAMU) is gratefully acknowledged under the grant number MUNI/J/0007/2021. We acknowledge CF CryoEM and CF NMR of CIISB, Instruct-CZ Centre, supported by MEYS CR (LM2023042) and European Regional Development Fund-Project „UP CIISB" (No. CZ.02.1.01/0.0/0.0/18_046/0015974). CzechNanoLab project LM2023051 funded by MEYS CR is gratefully acknowledged for the financial support of the XPS measurements at CEITEC Nano Research Infrastructure. This publication was supported by the project Quantum materials for applications in sustainable technologies (QM4ST), CZ.02.01.01/00/22_008/0004572 by Program J. A. Commenius, call Excellent Research. This research was supported by the Ministry of Education Youth and Sports of the Czech Republic - program DKRVO (RP/CPS/2024-28/002).

Appendix A. Supplementary data

Supplementary data to this article can be found online at https://doi.org/10.1016/j.micromeso.2024.113371.

Data availability

The link to the data is given in the manuscript.

References

[1] M. Faustini, L. Nicole, E. Ruiz-Hitzky, C. Sanchez, History of organic–inorganic hybrid materials: prehistory, art, science, and advanced applications, Adv. Funct. Mater. 28 (2018) 1704158, https://doi.org/10.1002/adfm.201704158.
[2] A. Erigoni, U. Diaz, Porous silica-based organic-inorganic hybrid catalysts: a review, Catalysts 11 (2021) 79, https://doi.org/10.3390/catal11010079.
[3] A. Styskalik, D. Skoda, C. Barnes, J. Pinkas, The power of non-hydrolytic sol-gel chemistry: a review, Catalysts 7 (2017) 168–210, https://doi.org/10.3390/catal7060168.
[4] P.H. Mutin, A. Vioux, Nonhydrolytic processing of oxide-based materials: simple routes to control homogeneity, morphology, and nanostructure, Chem. Mater. 21 (2009) 582–596, https://doi.org/10.1021/cm802348c.
[5] D.P. Debecker, P.H. Mutin, Non-hydrolytic sol-gel routes to heterogeneous catalysts, Chem. Soc. Rev. 41 (2012) 3624–3650, https://doi.org/10.1039/C2CS15330K.
[6] D.P. Debecker, V. Hulea, P.H. Mutin, Mesoporous mixed oxide catalysts via non-hydrolytic sol–gel: a review, Appl. Catal. Gen. 451 (2013) 192–206, https://doi.org/10.1016/j.apcata.2012.11.002.
[7] V. Lafond, P.H. Mutin, A. Vioux, Control of the texture of Titania−Silica mixed oxides prepared by nonhydrolytic Sol−Gel, Chem. Mater. 16 (2004) 5380–5386, https://doi.org/10.1021/cm0490569.
[8] V. Smeets, A. Styskalik, D.P. Debecker, Non-hydrolytic sol–gel as a versatile route for the preparation of hybrid heterogeneous catalysts, J. Sol. Gel Sci. Technol. 97 (2021) 505–522, https://doi.org/10.1007/s10971-021-05486-1.
[9] A. Styskalik, I. Kordoghli, C. Poleunis, A. Delcorte, C. Aprile, L. Fusaro, D.P.D. P. Debecker, Highly porous hybrid metallosilicate materials prepared by non-hydrolytic sol-gel: hydrothermal stability and catalytic properties in ethanol dehydration, Microporous Mesoporous Mater. 297 (2020) 110028, https://doi.org/10.1016/j.micromeso.2020.110028.
[10] A. Styskalik, I. Kordoghli, C. Poleunis, A. Delcorte, Z. Moravec, L. Simonikova, V. Kanicky, C. Aprile, L. Fusaro, D.P. Debecker, Hybrid mesoporous aluminosilicate catalysts obtained by non-hydrolytic sol–gel for ethanol dehydration, J. Mater. Chem. A 8 (2020) 23526–23542, https://doi.org/10.1039/D0TA07016E.
[11] P. Machac, A. Styskalik, Z. Moravec, J. Pinkas, Non-hydrolytic sol-gel synthesis of zirconium phosphonates with controlled mesoporosity, Microporous Mesoporous Mater. 362 (2023) 112787, https://doi.org/10.1016/j.micromeso.2023.112787.
[12] P. Machac, J.G. Alauzun, A. Styskalik, D.P. Debecker, P.H. Mutin, J. Pinkas, Synthesis of high surface area aluminophosphate and -phosphonate xerogels by non-hydrolytic sol-gel reactions, Microporous Mesoporous Mater. 311 (2021), https://doi.org/10.1016/j.micromeso.2020.110682.
[13] M.A. Ullmann, J.H.Z. dos Santos, Deactivation study of zirconocene immobilization into Lewis acid and dual-shell silicas prepared by a nonhydrolytic sol-gel method, J. Catal. 378 (2019) 226–237, https://doi.org/10.1016/j.jcat.2019.08.040.
[14] M.A. Ullmann, J.H.Z. dos Santos, Zirconocene immobilization into organic-inorganic dual-shell silicas prepared by the nonhydrolytic sol-gel method for polyethylene production, J. Catal. 385 (2020) 30–43, https://doi.org/10.1016/j.jcat.2020.03.001.
[15] L.B. Capeletti, M. do Carmo Martins Alves, M.B. Cardoso, J.H.Z. dos Santos, Hybrid silica based catalysts prepared by the encapsulation of zirconocene compound via non-hydrolytic sol-gel method for ethylene polymerization, Appl. Catal. Gen. 560 (2018) 225–235, https://doi.org/10.1016/j.apcata.2018.03.013.
[16] V. Smeets, L. Ben Mustapha, J. Schnee, E.M. Gaigneaux, D.P. Debecker, Mesoporous SiO2-TiO2 epoxidation catalysts: tuning surface polarity to improve performance in the presence of water, Mol. Catal. 452 (2018) 123–128, https://doi.org/10.1016/j.mcat.2018.04.011.
[17] W. Cho, M.S. Shin, S. Hwang, H. Kim, M. Kim, J.G. Kim, Y. Kim, Tertiary amines: a new class of highly efficient organocatalysts for CO2 fixations, J. Ind. Eng. Chem. 44 (2016) 210–215, https://doi.org/10.1016/j.jiec.2016.09.015.
[18] W. Natongchai, J.A. Luque-Urrutia, C. Phungpanya, M. Solà, V. D'Elia, A. Poater, H. Zipse, Cycloaddition of CO 2 to epoxides by highly nucleophilic 4-aminopyridines: establishing a relationship between carbon basicity and catalytic performance by experimental and DFT investigations, Org. Chem. Front. 8 (2021) 613–627, https://doi.org/10.1039/D0QO01327G.
[19] S. Ryu, A density functional study of amine catalysts for CO 2 fixation into cyclic carbonates, Bull. Kor. Chem. Soc. 40 (2019) 1033–1038, https://doi.org/10.1002/bkcs.11876.
[20] K.R. Roshan, R.A. Palissery, A.C. Kathalikkattil, R. Babu, G. Mathai, H.-S. Lee, D.-W. Park, A computational study of the mechanistic insights into base catalysed synthesis of cyclic carbonates from CO 2 : bicarbonate anion as an active species, Catal. Sci. Technol. 6 (2016) 3997–4004, https://doi.org/10.1039/C5CY01902H.
[21] R. Azzouz, V. Contreras Moreno, C. Herasme-Grullon, V. Levacher, L. Estel, A. Ledoux, S. Derrouiche, F. Marsais, L. Bischoff, Efficient conversion of epoxides into carbonates with CO2 and a single organocatalyst: laboratory and kilogram-scale experiments, Synlett 31 (2020) 183–188, https://doi.org/10.1055/s-0039-1691405.
[22] A. Samikannu, L.J. Konwar, P. Mäki-Arvela, J.-P. Mikkola, Renewable N-doped active carbons as efficient catalysts for direct synthesis of cyclic carbonates from epoxides and CO2, Appl. Catal. B Environ. 241 (2019) 41–51, https://doi.org/10.1016/j.apcatb.2018.09.019.
[23] T.Q. Bui, L.J. Konwar, A. Samikannu, D. Nikjoo, J.-P. Mikkola, Mesoporous melamine-formaldehyde resins as efficient heterogeneous catalysts for continuous synthesis of cyclic carbonates from epoxides and gaseous CO 2, ACS Sustain. Chem. Eng. 8 (2020) 12852–12869, https://doi.org/10.1021/acssuschemeng.0c03123.

[24] R. Luo, Y. Yang, K. Chen, X. Liu, M. Chen, W. Xu, B. Liu, H. Ji, Y. Fang, Tailored covalent organic frameworks for simultaneously capturing and converting CO 2 into cyclic carbonates, J. Mater. Chem. A 9 (2021) 20941–20956, https://doi.org/10.1039/D1TA05428G.
[25] S. Yan, W. Li, D. He, G. He, H. Chen, Recent research progress of metal-organic frameworks (MOFs) based catalysts for CO2 cycloaddition reaction, Mol. Catal. 550 (2023) 113608, https://doi.org/10.1016/j.mcat.2023.113608.
[26] G. Li, S. Dong, P. Fu, Q. Yue, Y. Zhou, J. Wang, Synthesis of porous poly(ionic liquid)s for chemical CO 2 fixation with epoxides, Green Chem. 24 (2022) 3433–3460, https://doi.org/10.1039/D2GC00324D.
[27] A. Hajipour, Y. Heidari, G. Kozehgary, Silica-grafted basic amino acids as environmentally benign catalysts for the solventless synthesis of cyclic carbonates from epoxides and CO2 under metal-free and halide-free conditions, Synlett 27 (2016) 929–933, https://doi.org/10.1055/s-0035-1561309.
[28] M. Sankar, T.G. Ajithkumar, G. Sankar, P. Manikandan, Supported imidazole as heterogeneous catalyst for the synthesis of cyclic carbonates from epoxides and CO2, Catal. Commun. 59 (2015) 201–205, https://doi.org/10.1016/j.catcom.2014.10.026.
[29] R. Srivastava, D. Srinivas, P. Ratnasamy, Sites for CO2 activation over amine-functionalized mesoporous Ti(Al)-SBA-15 catalysts, Microporous Mesoporous Mater. 90 (2006) 314–326, https://doi.org/10.1016/j.micromeso.2005.10.043.
[30] T.P. Nguyen, P. Hesemann, T.M. Linh Tran, J.J.E.E. Moreau, Nanostructured polysilsesquioxanes bearing amine and ammonium groups by micelle templating using anionic surfactants, J. Mater. Chem. 20 (2010) 3910, https://doi.org/10.1039/b925352a.
[31] G. Zhou, T. Simerly, L. Golovko, I. Tychinin, V. Trachevsky, Y. Gomza, A. Vasiliev, Highly functionalized bridged silsesquioxanes, J. Sol. Gel Sci. Technol. 62 (2012) 470–482, https://doi.org/10.1007/s10971-012-2751-5.
[32] K.O. Ojo, L.V. Golovko, Y.P. Gomza, A.N. Vasiliev, Mesoporous silsesquioxanes with high contents of surface amine groups, Silicon 4 (2012) 189–195, https://doi.org/10.1007/s12633-012-9122-2.
[33] S. El Hankari, B. Motos-Pérez, P. Hesemann, A. Bouhaouss, J.J.E. Moreau, Pore size control and organocatalytic properties of nanostructured silica hybrid materials containing amino and ammonium groups, J. Mater. Chem. 21 (2011) 6948, https://doi.org/10.1039/c1jm10422e.
[34] E.A. Prasetyanto, M.B. Ansari, B.-H. Min, S.-E. Park, Melamine tri-silsesquioxane bridged periodic mesoporous organosilica as an efficient metal-free catalyst for CO2 activation, Catal. Today 158 (2010) 252–257, https://doi.org/10.1016/j.cattod.2010.03.081.
[35] N. Velikova, I. Spassova, Amine functionalized mesoporous hybrid materials: influence of KCl and xylene on the textural characteristics and CO2 sorption, J. Sol. Gel Sci. Technol. 91 (2019) 374–384, https://doi.org/10.1007/s10971-019-04998-1.
[36] D.V. Quang, A. Dindi, K. Al-Ali, M.R.M. Abu-Zahra, Template-free amine-bridged silsesquioxane with dangling amino groups and its CO 2 adsorption performance, J. Mater. Chem. A 6 (2018) 23690–23702, https://doi.org/10.1039/C8TA05106B.
[37] O. Esam, G. Zhou, A. Vasiliev, Bridged mesoporous silsesquioxanes as potential CO2 adsorbents, J. Sol. Gel Sci. Technol. 74 (2015) 740–747, https://doi.org/10.1007/s10971-015-3657-9.
[38] A. Kuvayskaya, B. Lotsi, R. Mohseni, A. Vasiliev, Mesoporous adsorbents for perfluorinated compounds, Microporous Mesoporous Mater. 305 (2020) 110374, https://doi.org/10.1016/j.micromeso.2020.110374.
[39] N. Velikova, Y. Vueva, Y. Ivanova, I. Salvado, M. Fernandes, P. Vassileva, R. Georgieva, A. Detcheva, Synthesis and characterization of sol–gel mesoporous organosilicas functionalized with amine groups, J. Non-Cryst. Solids 378 (2013) 89–95, https://doi.org/10.1016/j.jnoncrysol.2013.06.024.
[40] Z. Wu, L. You, H. Xiang, Y. Jiang, Comparison of dye adsorption by mesoporous hybrid gels: understanding the interactions between dyes and gel surfaces, J. Colloid Interface Sci. 303 (2006) 346–352, https://doi.org/10.1016/j.jcis.2006.08.018.
[41] A. Styskalik, D. Skoda, Z. Moravec, J.G. Abbott, C.E. Barnes, J. Pinkas, Synthesis of homogeneous silicophosphate xerogels by non-hydrolytic condensation reactions, Microporous Mesoporous Mater. 197 (2014) 204–212, https://doi.org/10.1016/j.micromeso.2014.06.019.
[42] A. Styskalik, D. Skoda, Z. Moravec, M. Babiak, C.E. Barnes, J. Pinkas, Control of micro/mesoporosity in non-hydrolytic hybrid silicophosphate xerogels, J. Mater. Chem. A 3 (2015) 7477–7487, https://doi.org/10.1039/C4TA06823H.
[43] A. Styskalik, D. Skoda, J. Pinkas, S. Mathur, Non-hydrolytic synthesis of titanosilicate xerogels by acetamide elimination and their use as epoxidation catalysts, J. Sol. Gel Sci. Technol. 63 (2012) 463–472, https://doi.org/10.1007/s10971-012-2808-5.
[44] M. Jansen, E. Guenther, Oxide gels and ceramics prepared by a nonhydrolytic sol-gel process, Chem. Mater. 7 (1995) 2110–2114, https://doi.org/10.1021/cm00059a019.
[45] J. Caruso, C. Roger, F. Schwertfeger, M.J. Hampden-Smith, A.L. Rheingold, G. Yap, Solvent-dependent ester elimination and ligand exchange reactions between trimethylsilyl acetate and tin(IV) tetra-tert-butoxide, Inorg. Chem. 34 (1995) 449–453, https://doi.org/10.1021/ic00106a006.
[46] I. Slavchev, J.S. Ward, K. Rissanen, G.M. Dobrikov, S. Simeonov, Base-promoted direct amidation of esters: beyond the current scope and practical applications, RSC Adv. 12 (2022) 20555–20562, https://doi.org/10.1039/D2RA03524C.
[47] M. Thommes, K. Kaneko, A.V. Neimark, J.P. Olivier, F. Rodriguez-Reinoso, J. Rouquerol, K.S.W. Sing, Physisorption of gases, with special reference to the evaluation of surface area and pore size distribution (IUPAC Technical Report), Pure Appl. Chem. 87 (2015) 1051–1069, https://doi.org/10.1515/pac-2014-1117.
[48] L.E. Dunlap, D.E. Olson, Reaction of N , N -dimethyltryptamine with dichloromethane under common experimental conditions, ACS Omega 3 (2018) 4968–4973, https://doi.org/10.1021/acsomega.8b00507.
[49] J.E. Gordon, Fused organic salts. III. 1a chemical stability of molten tetra-n-alkylammonium salts. Medium effects on thermal R 4 N + X - decomposition. RBr + I - = RI + Br - equilibrium constant in fused salt medium, J. Org. Chem. 30 (1965) 2760–2763, https://doi.org/10.1021/jo01019a060.
[50] S. Kaewsai, S. Del Gobbo, V. D'Elia, Synthesis of bifunctional catalysts for the cycloaddition of CO 2 to epoxides through an epoxide-driven strategy, ChemCatChem 16 (2024), https://doi.org/10.1002/cctc.202301713.
[51] R. Jin, H. Xu, J. Easa, A. Chapero-Planell, C.P. O'Brien, Cycloaddition of CO 2 to epichlorohydrin over pyridine, vinylpyridine, and poly(vinylpyridine): the influence of steric crowding on the reaction mechanism, J. Phys. Chem. C 127 (2023) 1441–1454, https://doi.org/10.1021/acs.jpcc.2c08516.
[52] Y.G. Ko, S.S. Shin, U.S. Choi, Primary, secondary, and tertiary amines for CO2 capture: designing for mesoporous CO2 adsorbents, J. Colloid Interface Sci. 361 (2011) 594–602, https://doi.org/10.1016/j.jcis.2011.03.045.
[53] L. O'Hare, B. Parbhoo, S.R. Leadley, Development of a methodology for XPS curve-fitting of the Si 2p core level of siloxane materials, Surf. Interface Anal. 36 (2004) 1427–1434, https://doi.org/10.1002/sia.1917.
[54] G. Beamson, D. Briggs, High Resolution XPS of Organic Polymers: the Scienta ESCA300 Database, Wiley, 1992. https://books.google.cz/books?id=SIl5QgAACAAJ.
[55] B. Smith, Infrared Spectral Interpretation, CRC Press, 2018, https://doi.org/10.1201/9780203750841.
[56] P. Larkin, Infrared and Raman Spectroscopy: Principles and Spectral Interpretation, Elsevier, 2017.
[57] M. Handke, A. Kowalewska, Siloxane and silsesquioxane molecules - precursors for silicate materials, Spectrochim. Acta Part A Mol. Biomol. Spectrosc. (2011) 749–757, https://doi.org/10.1016/j.saa.2010.08.049. Elsevier.
[58] A. Nuhnen, C. Janiak, A practical guide to calculate the isosteric heat/enthalpy of adsorption via adsorption isotherms in metal–organic frameworks, MOFs, Dalt. Trans. 49 (2020) 10295–10307, https://doi.org/10.1039/D0DT01784A.
[59] D.D. Do, Adsorption Analysis: Equilibria and Kinetics, Imperial College Press, London, 1998.
[60] A. Samanta, A. Zhao, G.K.H. Shimizu, P. Sarkar, R. Gupta, Post-Combustion CO 2 capture using solid sorbents: a review, Ind. Eng. Chem. Res. 51 (2012) 1438–1463, https://doi.org/10.1021/ie200686q.
[61] S. Soll, Q. Zhao, J. Weber, J. Yuan, Activated CO 2 sorption in mesoporous imidazolium-type poly(ionic liquid)-based polyampholytes, Chem. Mater. 25 (2013) 3003–3010, https://doi.org/10.1021/cm4009128.
[62] N.F.A. van der Vegt, V.A. Kusuma, B.D. Freeman, Basis of solubility versus T C correlations in polymeric gas separation membranes, Macromolecules 43 (2010) 1473–1479, https://doi.org/10.1021/ma9024653.
[63] V.M. Shah, B.J. Hardy, S.A. Stern, Solubility of carbon dioxide, methane, and propane in silicone polymers: effect of polymer side chains, J. Polym. Sci., Part B: Polym. Phys. 24 (1986) 2033–2047, https://doi.org/10.1002/polb.1986.090240910.
[64] F. Raganati, F. Miccio, P. Ammendola, Adsorption of carbon dioxide for post-combustion capture: a review, Energy Fuel. 35 (2021) 12845–12868, https://doi.org/10.1021/acs.energyfuels.1c01618.
[65] N. Velikova, I. Spassova, Bifunctional mesoporous hybrid sol-gel prepared silicas for CO2 adsorption, J. Sol. Gel Sci. Technol. 100 (2021) 326–340, https://doi.org/10.1007/s10971-021-05641-8.
[66] V.B. Saptal, B. Nanda, K.M. Parida, B.M. Bhanage, Fabrication of amine and zirconia on MCM-41 as acid–base catalysts for the fixation of carbon dioxide, ChemCatChem 9 (2017) 4105–4111, https://doi.org/10.1002/cctc.201700656.
[67] F. Pourhassan, R. Khalifeh, H. Eshghi, Well dispersed gold nanoparticles into the multi amine functionalized SBA-15 for green chemical fixation of carbon dioxide to cyclic carbonates under solvent free conditions, Fuel 287 (2021) 119567, https://doi.org/10.1016/j.fuel.2020.119567.
[68] A. Bansal, R. Sharma, P. Mohanty, Nanocasted polytriazine-SBA-16 mesoporous composite for the conversion of CO2 to cyclic carbonates, J. CO2 Util. 40 (2020) 101189, https://doi.org/10.1016/j.jcou.2020.101189.
[69] Y. Ye, D. Li, P. Xu, J. Sun, B-Doped and NH 2 -functionalized SBA-15 with hydrogen bond donor groups for effective catalysis of CO 2 cycloaddition to epoxides, Inorg. Chem. Front. 7 (2020) 3636–3645, https://doi.org/10.1039/D0QI00703J.
[70] X. Zhang, N. Zhao, W. Wei, Y. Sun, Chemical fixation of carbon dioxide to propylene carbonate over amine-functionalized silica catalysts, Catal. Today 115 (2006) 102–106, https://doi.org/10.1016/j.cattod.2006.02.028.
[71] T. Sakai, Y. Tsutsumi, T. Ema, Highly active and robust organic–inorganic hybrid catalyst for the synthesis of cyclic carbonates from carbon dioxide and epoxides, Green Chem. 10 (2008) 337, https://doi.org/10.1039/b718321f.
[72] K.M.K. Yu, I. Curcic, J. Gabriel, H. Morganstewart, S.C. Tsang, Catalytic coupling of CO 2 with epoxide over supported and unsupported amines, J. Phys. Chem. A 114 (2010) 3863–3872, https://doi.org/10.1021/jp906365g.
[73] J. Steinbauer, L. Longwitz, M. Frank, J. Epping, U. Kragl, T. Werner, Immobilized bifunctional phosphonium salts as recyclable organocatalysts in the cycloaddition of CO 2 and epoxides, Green Chem. 19 (2017) 4435–4445, https://doi.org/10.1039/C7GC01782K.
[74] M. Alonso de la Peña, M. Balas, J. Kong, R. Villanneau, L. Christ, A. Tuel, F. Launay, Towards metal-free supported quaternary ammonium halide catalysts for an optimized cycloaddition of CO 2 onto styrene oxide, Catal. Sci. Technol. 14 (2024) 1305–1317, https://doi.org/10.1039/D3CY01551C.